DESY 18-0YY ISSN 0418-9833
February 2, 2018
Draft version 2.0

Combination and QCD analysis of beauty and charm production cross section measurements in deep inelastic ep scattering at HERA

The H1 and ZEUS Collaborations

Abstract

Measurements of open charm and beauty production cross sections in deep inelastic ep scattering at HERA from the H1 and ZEUS Collaborations are combined. Reduced cross sections are obtained in the kinematic range of negative four-momentum transfer squared of the photon 2.5 GeV$^2 \leq Q^2 \leq$ 2000 GeV^2 and Bjorken scaling variable $3 \cdot 10^{-5} \leq x_{\mathrm{Bj}} \leq 5 \cdot 10^{-2}$. The combination method accounts for the correlations of the statistical and systematic uncertainties among the different data sets. Perturbative QCD calculations are compared to the combined data. A next-to-leading order QCD analysis is performed using these data together with the combined inclusive deep inelastic scattering cross sections from HERA. The running charm and beauty quark masses are determined as $m_c(m_c) = 1.290^{+0.046}_{-0.041}(\mathrm{exp/fit})^{+0.062}_{-0.014}(\mathrm{model})^{+0.003}_{-0.031}(\mathrm{parameterisation})$ GeV and $m_b(m_b) = 4.049^{+0.104}_{-0.109}(\mathrm{exp/fit})^{+0.090}_{-0.032}(\mathrm{model})^{+0.001}_{-0.031}(\mathrm{parameterisation})$ GeV.

1 Introduction

Measurements of open charm and beauty production in neutral current (NC) deep inelastic electron[1]–proton scattering (DIS) at HERA provide important input for tests of the theory of strong interactions, quantum chromodynamics (QCD). Measurements at HERA [1–24] have shown that heavy flavour production in DIS proceeds predominantly via the boson-gluon-fusion process, $\gamma g \rightarrow Q\overline{Q}$, where Q is the heavy quark. The cross section therefore depends strongly on the gluon distribution in the proton and the heavy quark mass. This mass provides a sufficiently high scale for the applicability of perturbative QCD (pQCD). However, other hard scales are also present in this process: the transverse momenta of the outgoing quarks and the negative four momentum squared, Q^2, of the exchanged photon. The presence of several hard scales complicates the calculation of heavy flavour production in pQCD. Different approaches have been developed to cope with the multiple scale problem inherent in this process. In this paper, the massive fixed-flavour-number-scheme (FFNS) [25–33] and different implementations of the variable-flavour-number scheme (VFNS) [34–37] are considered.

At HERA different flavour tagging methods are applied for charm and beauty cross section measurements: the full reconstruction of D or $D^{*\pm}$ mesons [1, 2, 4–6, 10–12, 15, 17, 20–22], which is almost exclusively sensitive to charm production; the lifetime of heavy flavoured hadrons [7–9, 14, 23] and their semi-leptonic decays [13, 16, 19], both enabling the measurement of the charm and beauty cross section simultaneously. In general, the different methods explore different regions of the heavy quark phase space and show different dependencies on sources of systematic uncertainties. Therefore, by using different tagging techniques a more complete picture of heavy flavour production is obtained.

In this paper a simultaneous combination of charm and beauty production cross section measurements is presented. This analysis is an extension of the previous H1 and ZEUS combination of charm measurements in DIS [38], including new charm and beauty data [13,14,16,19,21–23] and extracting combined beauty cross sections for the first time. As a result, a single consistent dataset from HERA of reduced charm and beauty cross sections in DIS is obtained, including all cross-correlations. This dataset covers the kinematic range of photon virtuality $2.5 \leq Q^2 \leq 2000$ GeV^2 and Bjorken scaling variable $3 \times 10^{-5} \leq x_{\mathrm{Bj}} \leq 5 \times 10^{-2}$.

The procedure used is based on that described in [38–42]. The correlated systematic uncertainties and the normalisation of the different measurements are accounted for such that one consistent data set is obtained. Since different experimental techniques of charm and beauty tagging have been employed using different detectors and methods of kinematic reconstruction, this combination leads to a significant reduction of statistical and systematic uncertainties. The simultaneous combination of charm and beauty cross section measurements reduces the correlations between them and hence also the uncertainties. The combined reduced charm cross sections of the previous analysis [38] are superseded by the new results presented in this paper.

The combined data are compared to theoretical predictions obtained in the FFNS at next-to-leading order (NLO, $O(\alpha_s^2)$) QCD using HERAPDF2.0 [43], ABKM09 [26,27] and ABMP16 [29] parton distribution functions (PDFs), and to approximate next-to-next-to-leading order (NNLO, $O(\alpha_s^3)$) using ABMP16 [29] PDFs. In addition QCD calculations in the RTOPT variable-flavour-number scheme (VFNS) at NLO and approximate NNLO [34] are compared with the

[1] In this paper the term 'electron' denotes both electron and positron if not stated otherwise.

data. The NLO calculations are at $O(\alpha_s^2)$ except for the massless parts the coefficient functions, which are at $O(\alpha_s)$; the NNLO calculations split identically but are one order of α_s higher. A comparison is also made to predictions of two variants of the FONLL-C scheme [35, 36] ($O(\alpha_s^3)$ (NNLO) in the PDF evolution, $O(\alpha_s^2)$ in all coefficient functions): the default FONLL-C scheme, which includes next-to-leading-log (NLL) resummation of quasi-collinear final state gluon radiation, and a variant which includes NLL low-x resummation in the PDFs and the matrix elements (NLLsx) [37] in addition.

The new data are subjected to a QCD analysis together with inclusive DIS cross section data from HERA [43] allowing for the determination at NLO of the running charm and beauty quark masses, as defined in the QCD Lagrangian in the modified minimum-subtraction ($\overline{\mathrm{MS}}$) scheme.

The paper is organised as follows. In section 2, the reduced heavy flavour cross section is defined and the theoretical framework is briefly introduced. The heavy flavour tagging methods, the data samples and the combination method are presented in section 3. The resulting reduced charm and beauty cross sections are presented in section 4 and in section 5 they are compared with theoretical calculations based on existing PDF sets and with existing predictions at NLO and at NNLO in the FFNS and VFNS. In section 6, the NLO QCD analysis is described and the measurement of the running masses of the charm and beauty quarks in the $\overline{\mathrm{MS}}$ scheme at NLO is presented. The conclusions are given in section 7.

2 Heavy flavour production in DIS

In this paper, charm and beauty production via NC deep inelastic ep scattering are considered. In the kinematic range explored by the analysis of the data presented here Q^2 is much smaller than M_Z^2, such that the virtual photon exchange dominates. Contributions from Z exchange and γZ interference are small and therefore neglected. The cross section for the production of a heavy flavour of type Q, with Q being either beauty, b, or charm, c, may then be written in terms of the heavy flavour contributions to the structure functions F_2 and F_L, $F_2^{\mathrm{Q\overline{Q}}}(x_{\mathrm{Bj}}, Q^2)$ and $F_L^{\mathrm{Q\overline{Q}}}(x_{\mathrm{Bj}}, Q^2)$, as

$$\frac{\mathrm{d}^2\sigma^{\mathrm{Q\overline{Q}}}}{\mathrm{d}x_{\mathrm{Bj}}\mathrm{d}Q^2} = \frac{2\pi\left(\alpha(Q^2)\right)^2}{x_{\mathrm{Bj}}Q^4}([1+(1-y)^2]F_2^{\mathrm{Q\overline{Q}}}(x_{\mathrm{Bj}}, Q^2) - y^2 F_{\mathrm{L}}^{\mathrm{Q\overline{Q}}}(x_{\mathrm{Bj}}, Q^2)) \; , \qquad (1)$$

where y denotes the lepton inelasticity. The superscripts $\mathrm{Q\overline{Q}}$ indicate the presence of a heavy quark pair in the final state. The cross section $\mathrm{d}^2\sigma^{\mathrm{Q\overline{Q}}}/\mathrm{d}x_{\mathrm{Bj}}\mathrm{d}Q^2$ is given at the Born level without QED and electroweak radiative corrections, except for the running electromagnetic coupling, $\alpha(Q^2)$.

In this paper, the results are presented in terms of reduced cross sections, defined as follows:

$$\begin{aligned} \sigma_{\mathrm{red}}^{\mathrm{Q\overline{Q}}} &= \frac{\mathrm{d}^2\sigma^{\mathrm{Q\overline{Q}}}}{\mathrm{d}x_{\mathrm{Bj}}\mathrm{d}Q^2} \cdot \frac{x_{\mathrm{Bj}}Q^4}{2\pi\alpha^2(Q^2)\,(1+(1-y)^2)} \\ &= F_2^{\mathrm{Q\overline{Q}}} - \frac{y^2}{1+(1-y)^2} F_{\mathrm{L}}^{\mathrm{Q\overline{Q}}}. \end{aligned} \qquad (2)$$

In the kinematic range addressed, the expected contribution from the exchange of longitudinally polarised photons, $F_{\mathrm{L}}^{\mathrm{Q\overline{Q}}}$, is small. In charm production it is expected to reach a few per cent at high y [45]. The structure functions $F_2^{\mathrm{Q\overline{Q}}}$ and $F_{\mathrm{L}}^{\mathrm{Q\overline{Q}}}$ are always calculated to the same order (mostly $O(\alpha_s^2)$) in all calculations explicitly performed in this paper.

2.1 Theory of heavy flavour production

Several theoretical approaches can be used for describing heavy flavour production in DIS. At values of Q^2 not very much larger than m_{Q}, heavy flavours are produced predominantly dynamically by the photon-gluon-fusion process. The creation of a $\mathrm{Q\overline{Q}}$ pair sets a lower limit of $2m_{\mathrm{Q}}$ to the mass of the hadronic final state. This low mass cutoff affects the kinematics and the higher order corrections in the phase space accessible at HERA. Therefore, a careful theoretical treatment of the heavy flavour masses is mandatory for the pQCD analysis of heavy flavour production as well as for the determination of the PDFs of the proton from data including heavy flavours.

In this paper, the FFNS is used for pQCD calculations for the corrections of measurements to the full phase space and in the QCD fits. In this scheme, heavy quarks are always treated as massive and therefore are not considered as partons in the proton. The number of (light) active flavours in the PDFs, n_f, is set to three and heavy quarks are produced only in the hard scattering process. The leading order (LO) contribution to heavy flavour production ($O(\alpha_s)$ in the coefficient functions) is the boson-gluon-fusion process. The NLO massive coefficient functions using on-shell mass renormalisation (pole masses) were calculated in [25] and adopted by many global QCD analysis groups [28, 30–32], providing PDFs derived from this scheme. They were extended to the $\overline{\mathrm{MS}}$ scheme in [27], using scale dependent (running) heavy quark masses. The advantage of performing heavy flavour calculations in the $\overline{\mathrm{MS}}$ scheme are reduced scale uncertainties and improved theoretical precision of the mass definition [24, 33]. In all FFNS heavy flavour calculations presented in this paper, the default renormalisation scale μ_r and factorisation scale μ_f are set to $\mu_r = \mu_f = \sqrt{Q^2 + 4m_{\mathrm{Q}}^2}$, where m_{Q} is the appropriate pole or running mass.

For the extraction of the combined reduced cross sections of beauty and charm production presented in this paper, the FFNS at NLO is used to calculate inclusive [25] and exclusive [46] quantities in the pole mass scheme. This is currently the only scheme for which exclusive NLO calculations are available.

The QCD analysis at NLO including the extraction of the heavy quark running masses is performed in the FFNS with the OPENQCDRAD programme [47] in the XFITTER (former HERAFITTER) framework [48]. In OPENQCDRAD, heavy quark production is calculated either using the $\overline{\mathrm{MS}}$ or the pole mass treatment of heavy quark masses. In this paper the $\overline{\mathrm{MS}}$ scheme is adopted.

Predictions from different variants of the VFNS are also compared to the data. The expectations from the NLO and approximate NNLO RTOPT [34] implementation as used for HERAPDF2.0 [43] are confronted with both the charm and beauty cross sections while the FONNL-C calculations [36, 37] are compared to the charm data only. In the VFNS, heavy quarks are treated as massive at small Q^2 up to $Q^2 \approx O(m_{\mathrm{Q}}^2)$ and as massless at $Q^2 \gg m_{\mathrm{Q}}^2$, with interpolation prescriptions between the two regimes which avoid double counting of common terms. In the FONLL-C calculations, the massive part of the charm coefficient functions is treated at NLO ($O(\alpha_s^2)$) while the massless part and the PDFs are treated at NNLO ($O(\alpha_s^2)$ and $O(\alpha_s^3)$, respectively). In addition to the default FONLL-C scheme a variant with NLL low-x resummation in the PDFs and matrix elements (NLLsx) [37] is considered.

3 Combination of H1 and ZEUS measurements

The different charm and beauty tagging methods exploited at HERA enable a comprehensive study of heavy flavour production in NC DIS.

Using fully reconstructed D or $D^{*\pm}$ mesons gives the best signal-to-background ratio for measurements of the charm production process. Although the branching ratios of beauty hadrons to D and $D^{*\pm}$ mesons are large, the contribution from beauty production to the observed D or $D^{*\pm}$ meson samples is small for several reasons. Firstly, beauty production is suppressed relative to charm production by a factor $1/4$ because of the quark's electric charge coupling to the photon. Secondly, the boson-gluon-fusion cross section depends on the invariant mass of the outgoing partons, $\hat{s}$, which has a threshold value of $4m_{\mathrm{Q}}^2$. Because the beauty quark mass, m_b, is about three times the charm quark mass, m_c, beauty production is significantly suppressed. Thirdly, in beauty production D and $D^{*\pm}$ mesons originate from the fragmentation of charm quarks that are produced by the weak decay of B mesons. Therefore the momentum fraction of the beauty quark carried by the D or $D^{*\pm}$ meson is small, so that the mesons mostly remain undetected.

Fully inclusive analyses based on the lifetime of the heavy flavoured mesons are sensitive to both charm and beauty production. Although the first two reasons given above for the suppression of beauty production relative to charm production also hold in this case, sensitivity to beauty production can be enhanced by several means. The proper lifetime of B mesons is about a factor of 2 to 3 that of D mesons on average [54]. Therefore, the charm and beauty contributions can be disentangled by using observables directly sensitive to the lifetime of the decaying heavy flavoured hadrons. The separation can be further improved by the simultaneous use of observables sensitive to the mass of the heavy flavoured hadron: the relative transverse momentum, $p_{\mathrm{T}}^{\mathrm{rel}}$, of the particle with lifetime information with respect to the flight direction of the decaying heavy flavoured hadron; the number of tracks with lifetime information; the invariant mass calculated from the charged particles attached to a secondary vertex candidate.

The analysis of lepton production is sensitive to semi-leptonic decays of both charm and beauty hadrons. When taking into account the fragmentation fractions of the heavy quarks as well as the fact that in beauty production leptons may originate both from the $b \to c$ and the $c \to s$ transition, the semi-leptonic branching fraction of B mesons is about twice that of D mesons [54]. Because of the large masses of B mesons and the harder fragmentation of beauty quarks compared to charm quarks, leptons originating directly from the B decays have on average higher momenta than those produced in D meson decays. Therefore the experimentally observed fraction of beauty induced leptons is enhanced relative to the observed charm induced fraction. Similar methods as outlined in the previous paragraph are then used to further facilitate the separation of the charm and beauty contribution on a statistical basis.

While the measurement of fully reconstructed D or $D^{*\pm}$ mesons yields the cleanest charm production sample, it suffers from small branching fractions and significant losses, because all particles from the D or $D^{*\pm}$ meson decay have to be measured. Fully inclusive and semi-inclusive lepton analyses, which are sensitive to both charm and beauty production, profit from larger branching fractions and better coverage in polar angle. They are however affected by a worse signal to background ratio and the large statistical correlations between charm and beauty measurements inherent to these methods.

3.1 Data samples

The H1 [49] and ZEUS [50] detectors were general purpose instruments which consisted of tracking systems surrounded by electromagnetic and hadronic calorimeters and muon detectors, ensuring close to 4π coverage of the ep interaction region. Both detectors were equipped with high-resolution silicon vertex detectors [51, 52].

The datasets included in the combination are listed in table 1. The data have been obtained from both the HERA I (in the years: 1992–2000) and HERA II (in the years: 2003–2007) data-taking periods. The combination includes measurements using different tagging techniques: the reconstruction of particular decays of D mesons [4, 6, 10, 12, 15, 20–22] (datasets $2-7, 9, 10$), the inclusive analysis of tracks exploiting lifetime information [14, 23] (datasets $1, 11$) and the reconstruction of electrons and muons from heavy-flavour semileptonic decays [13, 16, 19] (datasets $8, 12, 13$).

The datasets 1 to 8 have already been used in the previous combination [38] of charm cross section measurements, while the datasets 9 to 13 are included for the first time in this analysis. It is important to note that dataset 9 of the current analysis supersedes one dataset of the previous charm combination (dataset 8 in table 1 of [38]), because the earlier analysis was based on a subset of only about 30% of the final statistics collected during the HERA II running period.

For the inclusive lifetime analysis of reference [14] (dataset 1) the reduced cross sections $\sigma_{\rm red}^{c\bar{c}}$ and $\sigma_{\rm red}^{b\bar{b}}$ are taken directly from the publication. For all other measurements, the combination starts from the measured double differential visible cross sections $\sigma_{\rm vis,bin}$ in bins of Q^2 and either $x_{\rm Bj}$ or y, where the visibility is defined by the particular range of transverse momentum p_T and pseudorapidity[2] η of the D-meson, lepton or jet as given in the corresponding publications. In case of inclusive D meson cross sections, small beauty contributions as estimated in the corresponding papers are subtracted. All published visible cross section measurements include corrections for radiation of real photons from the incoming and outgoing lepton using the HERACLES programme [53]. QED corrections to the incoming and outgoing quarks are not considered. All cross sections are updated using the most recent hadron decay branching ratios [54].

3.2 Extrapolation of visible cross sections to $\sigma_{\rm red}^{\rm Q\overline{Q}}$

Except for data set 1 of table 1, for which only measurements expressed in the full phase space are available, the visible cross sections $\sigma_{\rm vis,bin}$ measured in a limited phase space are converted

[2] The pseudorapidity is defined as $\eta = -\ln\tan\frac{\Theta}{2}$ where the polar angle Θ is defined with respect to the proton direction.

to reduced cross sections $\sigma_{\rm red}^{\rm Q\overline{Q}}$ using a common theory. The reduced cross section of a heavy flavour Q at a reference $(x_{\rm Bj}, Q^2)$ point is extracted according to

$$\sigma_{\rm red}^{\rm Q\overline{Q}}(x_{\rm Bj}, Q^2) = \sigma_{\rm vis,bin} \frac{\sigma_{\rm red}^{\rm Q\overline{Q},th}(x_{\rm Bj}, Q^2)}{\sigma_{\rm vis,bin}^{\rm th}}. \tag{3}$$

The programme for heavy quark production in DIS HVQDIS [46] is used to calculate the theory predictions for $\sigma_{\rm red}^{\rm Q\overline{Q},th}(x_{\rm Bj}, Q^2)$ and $\sigma_{\rm vis,bin}^{\rm th}$ in the NLO FFNS. Since the ratio in equation (3) describes the extrapolation from the visible phase space in p_T and η of the heavy flavour tag to the full phase space, only the shape of the cross section predictions in p_T and η is relevant for the corrections, while theory uncertainties related to normalisation cancel.

In pQCD, $\sigma_{\rm red}^{\rm th}$ can be written as the convolution integral of the proton PDFs with the hard matrix elements. For the identification of heavy flavour production, however, specific particles used for tagging have to be measured in the hadronic final state. This requires that in the calculation of $\sigma_{\rm vis}^{\rm th}$, the convolution includes the proton PDFs, the hard matrix elements and the fragmentation functions. In the case of the HVQDIS programme non-perturbative fragmentation functions are used. The different forms of the convolution integrals for $\sigma_{\rm red}^{\rm th}$ and $\sigma_{\rm vis}^{\rm th}$ necessitates the consideration of different sets of theory parameters.

The following parameters are used consistently in these NLO calculations and are varied within the quoted limits to estimate the uncertainties in the predictions introduced by these parameters:

- The **renormalisation and factorisation scales** are taken as $\mu_r = \mu_f = \sqrt{Q^2 + 4m_{\rm Q}^2}$. The scales are varied simultaneously up or down by a factor of two.
- The **pole masses of the charm and beauty quarks** are set to $m_c = 1.50 \pm 0.15$ GeV, $m_b = 4.50 \pm 0.25$ GeV, respectively. These variations also affect the values of the renormalisation and factorisation scales.
- For the **strong coupling constant**, the value $\alpha_s^{n_f=3}(M_Z) = 0.105 \pm 0.002$ is chosen, which corresponds to $\alpha_s^{n_f=5}(M_Z) = 0.116 \pm 0.002$.
- The **proton PDFs** are described by a series of FFNS variants of the HERAPDF1.0 set [38, 41] at NLO determined within the XFITTER framework. No heavy flavour measurements were included in the determination of these PDF sets. These PDF sets are those used in the previous combination [38] which were calculated for $m_c = 1.5 \pm 0.15$ GeV, $\alpha_s^{n_f=3}(M_Z) = 0.105 \pm 0.002$ and a simultaneous variation of the renormalisation and factorisation scales up and down by a factor two. For the determination of the PDFs, the beauty quark mass was fixed at $m_b = 4.50$ GeV. The renormalisation and factorisation scales were set to $\mu_r = \mu_f = Q$ for the light flavours and to $\mu_r = \mu_f = \sqrt{Q^2 + 4m_{\rm Q}^2}$ for the heavy flavours. For all parameter settings considered, the HERAPDF1.0 set with the corresponding parameter setting is used. As a cross check of the extrapolation procedure, the cross sections are also evaluated with the 3-flavour NLO versions of the HERAPDF2.0 set (FF3A) [43]; the differences are found to be smaller than the PDF-related cross-section uncertainties.

For the calculation of $\sigma^{\rm th}_{\rm vis}$, assumptions have been made on the fragmentation of the heavy quarks into particular hadrons and, when necessary, on the subsequent decays of the heavy flavoured hadrons into the particles used for tagging. The fragmentation model for c quarks is based on the measurements by H1 [56] and ZEUS [57] and is used as described in detail in the previous charm combination [38]. It is only briefly summarised below.

In the calculation of $\sigma^{\rm th}_{\rm vis}$ the following settings and parameters are used in addition to those needed for $\sigma^{\rm th}_{\rm vis}$ and are varied within the quoted limits:

- The **charm fragmentation function** is described by the Kartvelishvili function [55] controlled by a single parameter α_K to describe the longitudinal fraction of the charm quark momentum transferred to the D or $D^{*\pm}$ meson. Depending on the invariant mass $\hat{s}$ of the outgoing parton system, different values of α_K and their uncertainties are used as measured at HERA [56,57] for $D^{*\pm}$ mesons. The variation of α_K as a function of $\hat{s}$ observed in $D^{*\pm}$ measurements has been adapted to the longitudinal fragmentation function of ground state D mesons not originating from $D^{*\pm}$ decays [38]. Transverse fragmentation is modelled by assigning to the charmed hadron a transverse momentum k_T with respect to the direction of the charmed quark with an average value of $\langle k_T \rangle = 0.35 \pm 0.15$ GeV [38].

- The **charm fragmentation fractions** of a charm quark into a specific charmed hadron and their uncertainties are taken from [60].

- The **beauty fragmentation function** is parameterised according to Peterson et al. [58] with $\varepsilon_b = 0.0035 \pm 0.0020$ [59].

- The **branching ratios of D and $D^{*\pm}$ mesons** into the specific decay channels analysed and their uncertainties are taken from [54].

- The **branching fractions of semi-leptonic decays** of heavy-quarks to a muon or electron and their uncertainties are taken from [54].

- The **decay spectra of leptons originating from charmed hadrons** are modelled according to [61].

- The **decay spectrum for beauty hadrons into leptons** are taken from the PYTHIA [62] Monte Carlo (MC) programme, mixing direct semi-leptonic decays and cascade decays through charm according to the measured branching ratios [54]. It is checked that the MC describes BELLE and BABAR data [63] well.

- When necessary for the extrapolation procedure, **parton level jets** are reconstructed using the same clustering algorithms as used on detector level, and the cross sections are corrected for jet hadronisation effects using corrections derived in the original papers [16, 23].[3]

While the central values for the extrapolation factors $\sigma^{\rm Q\overline{Q},th}_{\rm red}(x_{\rm Bj},Q^2)/\sigma^{\rm th}_{\rm vis,bin}$ (see equation 3) are obtained in the FFNS pole mass scheme at NLO, their uncertainties are calculated such that they should cover potential deviations from the unknown ‘true’ QCD result. The resulting

[3]Since no such corrections are provided in [16], an uncertainty of 5% is assigned to cover the untreated hadronisation effects [16].

reduced cross sections, which include these uncertainties, can thus be compared to calculations in any QCD scheme to any order provided these calculations include uncertainties for potential deviations from the ‘true’ result.

3.3 Combination method

The quantities to be combined are the reduced charm and beauty cross sections, $\sigma_{\rm red}^{c\bar{c}}$ and $\sigma_{\rm red}^{b\bar{b}}$, respectively. The combined cross sections are determined at common $(x_{\rm Bj}, Q^2)$ grid points. For $\sigma_{\rm red}^{c\bar{c}}$ the grid is chosen to be the same as in [38]. The results are given for a centre-of-mass energy of $\sqrt{s} = 318$ GeV. The results of the H1 inclusive lifetime analysis (dataset 1) are taken directly from the original measurement in the form of $\sigma_{\rm red}^{c\bar{c}}$ and $\sigma_{\rm red}^{b\bar{b}}$.When needed, these measurements are transformed to the common grid $(x_{\rm Bj}, Q^2)$ points using the NLO FFNS calculations [25]. The uncertainties on the resulting scaling factors are found to be negligible.

The combination is based on the χ^2 minimisation procedure [39] used previously [38, 40, 41, 43]. The total χ^2 is defined as

$$\chi^2_{\rm exp}(\boldsymbol{m}, \boldsymbol{b}) = \sum_e \left[\sum_i \frac{\left(m^i - \sum_j \gamma_j^{i,e} m^i b_j - \mu^{i,e}\right)^2}{(\mu^{i,e} \cdot \delta_{i,e,\rm stat})^2 + (m^i \cdot \delta_{i,e,\rm uncorr})^2} \right] + \sum_j {b_j}^2. \tag{4}$$

The three sums are running over the different input datasets e, listed in table 1, the $(x_{\rm Bj}, Q^2)$ grid points i, for which the measured cross sections $\mu^{i,e}$ are combined to the cross sections m^i, and the sources j of the shifts b_j in units of standard deviations of the correlated uncertainties. The correlated uncertainties comprise the correlated systematic uncertainties and the statistical correlation between the charm and beauty cross section measurements. The quantities $\gamma_j^{i,e}$, $\delta_{i,e,stat}$ and $\delta_{i,e,uncorr}$ denote the relative correlated systematic, relative statistical and relative uncorrelated systematic uncertainties, respectively. The components of the vectors $\boldsymbol{m}$ are the combined cross sections m^i while those of the vector $\boldsymbol{b}$ are the shifts b_j.

In the present analysis, the correlated and uncorrelated systematic uncertainties are predominantly of multiplicative nature, i.e. they are proportional to the expected cross sections m^i. The statistical uncertainties are mainly background dominated and thus are treated as constant. All experimental systematic uncertainties are treated as independent between H1 and ZEUS. For the datasets 1, 8 and 11 of table 1, statistical correlations between charm and beauty cross sections are accounted for as reported in the original papers. Where necessary, the statistical correlation factors are corrected to take into account differences in the kinematic region of the charm and beauty measurements (dataset 11) or binning schemes (dataset 1), using theoretical predictions calculated with the HVQDIS programme. The consistent treatment of the correlations of statistical and systematic uncertainties, including the correlations between the charm and beauty data sets where relevant, yields a significant reduction of the overall uncertainties of the combined data, as detailed in the following section.

4 Combined cross sections

The values of the combined cross sections $\sigma_{\rm red}^{c\bar{c}}$ and $\sigma_{\rm red}^{b\bar{b}}$, together with the statistical, the uncorrelated and correlated systematic and the total uncertainties, are listed in tables 2 and 3. A total of 209 charm and 57 beauty data points are combined simultaneously to obtain 52 reduced charm and 27 reduced beauty cross-section measurements. A χ^2 value of 149 for 187 degrees of freedom (d.o.f.) is obtained in the combination, indicating good consistency of the input data sets. The distribution of pulls of the 266 input data points with respect to the combined cross sections is presented in figure 1. It is consistent with a Gaussian around zero without any significant outliers. The observed width of the pull distribution is smaller than unity which indicates a conservative estimate of the systematic uncertainties.

There are 167 sources of correlated uncertainties in total. These are 71 experimental systematic sources, 16 sources due to the extrapolation procedure (including the uncertainties on the fragmentation fractions and branching ratios) and 80 statistical charm and beauty correlations. The sources of correlated systematic and extrapolation uncertainties are listed in the appendix in table A.1, together with the cross section shifts induced by the sources and the reduction factors of the uncertaintie, obtained as a result of the combination. Both quantities are given in units of σ of the original uncertainties. All shifts of the systematic sources with respect to their nominal values are smaller than 1.5σ. Several systematic uncertainties are reduced significantly - by up to factors of two or more. The reductions are due to the different heavy flavour tagging methods applied and to the fact that for a given process (beauty or charm production), an unique cross section is probed by the different measurements at a given (x_{Bj}, Q^2) point. Those uncertainties for which large reductions have been observed already in the previous analysis [38] are reduced to at least the same level in the current combination, some are further significantly reduced due to the inclusion of new precise data [21–23]. The shifts and reductions obtained for 80 statistical correlations between beauty and charm cross sections are not shown. Only small reductions in the range of 10% are observed and these reductions are independent of x_{Bj} and Q^2. The cross section tables of the combined data together with the full information on the uncertainties can be found elsewhere [64].

The combined reduced cross sections $\sigma_{\mathrm{red}}^{c\bar{c}}$ and $\sigma_{\mathrm{red}}^{b\bar{b}}$ are shown as a function of x_{Bj} in bins of Q^2 together with the input H1 and ZEUS data in figures 2 and 3, respectively. The combined cross sections are significantly more precise than any of the individual input data sets for charm as well as for beauty production. This is illustrated in figure 4, where the charm and beauty measurements for $Q^2 = 32$ GeV^2 are shown. The uncertainty of the combined reduced charm cross section is 9% on average and reaches values of about 5% and below in the region 12 GeV$^2 \leq Q^2 \leq 60$ GeV^2. The uncertainty of the combined reduced beauty cross section is about 25% on average and reaches about 15% at small x_{Bj} and 12 GeV$^2 \leq Q^2 < 200$ GeV^2.

In figure 5 the combined reduced charm cross sections of this analysis are compared to the results of the previously published combination [38]. Good consistency between the different combinations can be observed. The detailed analysis of the cross section measurements reveals a relative improvement in precision of about 20% on average with respect to the previous measurements. The improvement reaches about 30% in the range 7 GeV$^2 \leq Q^2 \leq 60$ GeV^2, where the newly added data sets (datasets 9 – 11 in table 1) contribute with high precision.

5 Comparison with theory predictions

The combined heavy flavour data are compared with calculations using various PDF sets. Predictions using the FFNS [25–32] and the VFNS [34–37] are considered, focussing on results using HERAPDF2.0 PDF sets. The data are also compared to FFNS predictions based on different variants of PDF sets at NLO and approximate NNLO provided by the ABM group [26, 29]. In the case of the VFNS, recent calculations of the NNPDF group based on the NNPDF3.1sx PDF set [37] at NNLO, which specifically aim for a better description of the DIS structure functions at small x_{Bj} and Q^2, are also confronted with the measurements. Calculations in the FFNS based on the HERAPDF2.0 FF3A PDF set will be considered as reference calculations in the subsequent parts of the paper.

5.1 FFNS predictions

In figures 6 and 7, theoretical predictions of the FFNS in the $\overline{\mathrm{MS}}$ running mass scheme are compared to the combined cross sections $\sigma_{\mathrm{red}}^{c\bar{c}}$ and $\sigma_{\mathrm{red}}^{b\bar{b}}$, respectively. The theoretical predictions are obtained within the open-source QCD fit framework for PDF determination XFITTER [48] (version 2.0.0), which uses the OPENQCDRAD (version 2.1) programme [47] for the cross section calculations. The running heavy flavour masses are set to the world average values [54] of $m_c(m_c) = 1.27 \pm 0.03$ GeV and $m_b(m_b) = 4.18 \pm 0.03$ GeV. The predicted reduced cross sections are calculated using the HERAPDF2.0 FF3A [43] and ABMP16 [29] NLO PDF sets using NLO $(O(\alpha_s^2))$ coefficient functions and the ABMP16 [29] NNLO PDF set using approximate NNLO coefficient functions. The charm data are also compared to NLO predictions based on the ABKM09 [26] NLO PDF set already used in the previous analysis [38] of combined charm data. This PDF set was determined using a charm quark mass of $m_c(m_c) = 1.18$ GeV. The PDF sets considered were extracted without explicitly using heavy flavour data from HERA with the exception of the ABMP16 set, in which the HERA charm data from the previous combination [38] and some of the beauty data [14, 23] have been included. For the predictions based on the HERAPDF2.0 FF3A set, theory uncertainties are given which are calculated by adding in quadrature the uncertainties from the PDF set, the simultaneous variation of μ_r and μ_f by a factor of two up and down and the variation of the quark masses within the quoted uncertainties.

The FFNS calculations reasonably describe the charm data (figure 6) although in the kinematic range where the data are very precise, the data show a x_{Bj} dependence somewhat steeper than predicted by the calculations. For the different PDF sets and QCD orders considered, the predictions are quite similar at larger Q^2 while some differences can be observed at smaller Q^2 or x_{Bj}. For beauty production (figure 7) the predictions are in good agreement with the data within the considerably larger experimental uncertainties.

The description of the charm production data is illustrated further in figure 8, which shows the ratios of the reduced cross sections for data, ABKM09 and ABMP16 at NLO and approximate NNLO with respect to the NLO reduced cross sections predicted in the FFNS using the HERAPDF2.0 FF3A set. For $Q^2 \geq 18$ GeV^2, the theoretical predictions are similar in the kinematic region accessible at HERA. In this region, the predictions based on the different PDF sets and orders are well within the theoretical uncertainties obtained for the HERAPDF2.0 FF3A set. Towards smaller Q^2 and x_{Bj}, some differences in the predictions become evident. In the region of 7 GeV$^2 \leq Q^2 \leq 120$ GeV^2, the theory tends to be below the data at small x_{Bj} and above the data at large x_{Bj}, independent of the PDF set and order used.

In figure 9, the corresponding ratios are shown for the beauty data. In the kinematic region accessible at HERA, the predictions are very similar. Within the experimental uncertainties, the data are well described by all calculations.

5.2 VFNS predictions

In figure 10, predictions of the RTOPT [34] NLO and approximate NNLO VFNS using the corresponding NLO and NNLO HERAPDF2.0 PDF sets are compared to the charm measurements. As in figure 8, the ratio of data and theory predictions to the reference calculations are shown. While the NLO VFNS predictions are in general consistent with both the data cross sections and the reference calculations, the approximate NNLO cross sections show somewhat larger differences, about 10% smaller than the reference cross sections in the region $12\ \mathrm{GeV}^2 \leq Q^2 \leq 120\ \mathrm{GeV}^2$. On the other hand, at $Q^2 \leq 7\ \mathrm{GeV}^2$ the x_{Bj}-slopes of the NNLO VFNS predictions tend to describe the data somewhat better than the reference calculations. Overall, the NLO and approximate NNLO VFNS predictions describe the data about equally well, but not better than the reference FFNS calculations.

In figure 11, the same ratios in the preceding paragraph are shown for beauty production. In the kinematic region accessible in DIS beauty production at HERA, the differences between the different calculations are small in comparison to the experimental uncertainties of the measurements.

The calculations considered so far in general show some tension in describing the x_{Bj}-slopes of the measured charm data over a large range in Q^2. Therefore the charm data are compared in figure 12 to recent calculations [37, 65] in the FONNL-C scheme with (NLLO+NLLsx) and without (NNLO) low-x resummation in both $O(\alpha_s^2)$ matrix elements and $O(\alpha_s^3)$ PDF evolution, using the NNPDF3.1sx framework, which aims for a better description of the structure functions at low x_{Bj} and Q^2. The charm data from the previous combination have already been used for the determination of the NNPDF3.1sx PDFs. Both calculations provide a better description of the x_{Bj}-shape of the measured charm cross sections for $Q^2 \leq 32\ \mathrm{GeV}^2$. However, the predictions lie significantly below the data in most of the phase space. This is especially the case for the NNLO+NLLsx calculations. Overall, the description is not improved with respect to the FFNS reference calculations.

5.3 Summary of the comparison to theoretical predictions

The comparison to data of the different predictions considered is summarised in table 4 in which the agreement with data is expressed in terms of χ^2 and the corresponding fit probabilities (p-values). The table also includes a comparison to the previous combined charm data [38]. The agreement of the various predictions with the charm cross section measurements of the current analysis is poorer than with the results of the previous combination, for which consistency between theory and data within the experimental uncertainties is observed for most of the calculations. As shown in section 4, the charm cross sections of the current analysis agree well with the previous measurement but have considerably smaller uncertainties due to the high precision data added. The observed changes in the χ^2-values are consistent with the improvement in data precision if the predictions do not describe reality. The tension observed between the central theory predictions and the charm data ranges from $\sim 3\sigma$ to more than 6σ, depending on the prediction. Among the calculations considered, the NLO FFNS calculations provide the best description of the charm data. For the beauty cross sections, good agreement of theory and data is observed within the large experimental uncertainties. In all cases, the effect of the PDF uncertainties on the χ^2 values is negligible.

6 QCD analysis

The combined beauty and charm data are used together with the combined HERA inclusive DIS data [43] to perform a QCD analysis in the FFNS in the $\overline{\text{MS}}$ scheme at NLO. The main focus of this analysis is the simultaneous determination of the running heavy quark masses $m_c(m_c)$ and $m_b(m_b)$. The theory description of the x_{Bj}-dependence of the reduced charm cross section is also investigated.

6.1 Theoretical formalism and settings

The analysis is performed with the XFITTER [48] programme, in which the scale evolution of partons is calculated through DGLAP equations [66] at NLO, as implemented in the QCDNUM programme [67]. The theoretical FFNS predictions for the HERA data are obtained using the OPENQCDRAD program [47] interfaced in the XFITTER framework. The number of active flavours is set to $n_f = 3$ at all scales. For the heavy flavour contributions the scales are set to $\mu_r = \mu_f = \sqrt{Q^2 + 4m_{\text{Q}}^2}$. The heavy-quark masses are left free in the fit unless stated otherwise. For the light-flavour contributions to the inclusive DIS cross sections, the pQCD scales are set to $\mu_r = \mu_f = Q$. The massless contribution to the longitudinal structure function F_{L} is calculated to $O(\alpha_s)$. The strong coupling strength is set to $\alpha_s^{n_f=3}(M_Z) = 0.106$, corresponding to $\alpha_s^{n_f=5}(M_Z) = 0.118$. In order to perform the analysis in the kinematic region where pQCD is usually assumed to be applicable, the Q^2 range of the inclusive HERA data is restricted to $Q^2 \geq Q^2_{\text{min}} = 3.5\ \text{GeV}^2$. No such cut is applied to the charm and beauty data, since the relevant scales $\mu_r^2 = \mu_f^2 = Q^2 + 4m_{\text{Q}}^2$ are above $3.5\ \text{GeV}^2$ for all measurements.

This theory setup is slightly different from that used for the original extraction [43] of HERAPDF2.0 FF3A. In contrast to the analysis presented here, HERAPDF2.0 FF3A was determined using the on-shell mass (pole-mass) scheme for the calculation of heavy quark production and F_{L} was calculated to $O(\alpha_s^2)$.

Perturbative QCD predictions were fit to the data using the same χ^2 definition as for fits to the inclusive DIS data (equation (32) in reference [43]. It includes an additional logarithmic term that is relevant when the estimated statistical and uncorrelated systematic uncertainties in the data are rescaled during the fit [68]. The correlated systematic uncertainties are treated through nuisance parameters.

The procedure for the determination of the PDFs follows the approach of HERAPDF2.0 [43]. At the starting scale $\mu_{\text{f},0}$, the density functions of a parton f of the proton are parametrised using the generic form:

$$xf(x) = Ax^B\,(1-x)^C\left(1 + Dx + Ex^2\right), \tag{5}$$

where x is the momentum fraction transferred to the struck parton in the infinite momentum frame of the incoming proton. The parametrised PDFs are the gluon distribution $xg(x)$, the valence quark distributions $xu_v(x)$ and $xd_v(x)$, and the u- and d-type antiquark distributions $x\overline{U}(x)$ and $x\overline{D}(x)$.

At the initial QCD evolution scale[4] $\mu_{f,0}^2 = 1.9$ GeV^2, the default parameterisation of the PDFs has the form:

$$
\begin{aligned}
xg(x) &= A_g x^{B_g} (1-x)^{C_g} - A'_g x^{B'_g} (1-x)^{C'_g}, \\
xu_v(x) &= A_{u_v} x^{B_{u_v}} (1-x)^{C_{u_v}} (1+E_{u_v} x^2), \\
xd_v(x) &= A_{d_v} x^{B_{d_v}} (1-x)^{C_{d_v}}, \\
x\overline{U}(x) &= A_{\overline{U}} x^{B_{\overline{U}}} (1-x)^{C_{\overline{U}}} (1+D_{\overline{U}} x), \\
x\overline{D}(x) &= A_{\overline{D}} x^{B_{\overline{D}}} (1-x)^{C_{\overline{D}}}.
\end{aligned}
\tag{6}
$$

The gluon density function, $xg(x)$, is different from equation (5), it includes an additional term $-A'_g x^{B'_g} (1-x)^{C'_g}$. The antiquark density functions, $x\overline{U}(x)$ and $x\overline{D}(x)$, are defined as $x\overline{U}(x) = x\overline{u}(x)$ and $x\overline{D}(x) = x\overline{d}(x) + x\overline{s}(x)$, where $x\overline{u}(x)$, $x\overline{d}(x)$, and $x\overline{s}(x)$ are the up, down, and strange antiquark distributions, respectively. The total quark density functions are $xU(x) = xu_v(x) + x\overline{U}(x)$ and $xD(X) = xd_v(x) + x\overline{D}(x)$. The sea antiquark distribution is defined as $x\Sigma(x) = x\overline{u}(x) + x\overline{d}(x) + x\overline{s}(x)$. The normalisation parameters A_{u_v}, A_{d_v}, and A_g are determined by the QCD sum rules. The B and B' parameters determine the PDFs at small x, and the C parameters describe the shape of the distributions as $x \to 1$. The parameter $C'_g = 25$ is fixed [69]. Additional constraints $B_{\overline{U}} = B_{\overline{D}}$ and $A_{\overline{U}} = A_{\overline{D}}(1 - f_s)$ are imposed to ensure the same normalisation for the xu and xd distributions as $x \to 0$. The strangeness fraction $f_s = x\overline{s}/(x\overline{d} + x\overline{s})$ is fixed to $f_s = 0.4$ as in the HERAPDF2.0 analysis [43].

A selection from the parameters in equation (5) is made by first fitting with all D and E parameters set to zero, and then including them one at a time in the fit. The improvement in the χ^2 of the fit is monitored. If χ^2 improves significantly, the parameter is added and the procedure is repeated until no further improvement is observed. This leads to the same 14 free PDF parameters as in the inclusive HERAPDF2.0 analysis [43].

The PDF uncertainties are estimated according to the general approach of HERAPDF2.0 [43], in which the experimental, model, and parameterisation uncertainties are taken into account. The experimental uncertainties are determined using the tolerance criterion of $\Delta\chi^2 = 1$. Model uncertainties arise from the variations of the strong coupling constant $\alpha_s^{n_f=3}(M_Z) = 0.106 \pm 0.0015$, the simultaneous variation of the factorisation and renormalisation scales up and down by a factor of two, the variation of the strangeness fraction $0.3 \leq f_s \leq 0.5$, and the value of 2.5 GeV$^2 \leq Q^2_{\rm min} \leq 5.0$ GeV^2 imposed on the inclusive HERA data. The parameterisation uncertainty is estimated by extending the functional form in equation (6) of all parton density functions with additional parameters D and E added one at a time. An additional parameterisation uncertainty is considered by using the functional form in equation (6) with $E_{u_v} = 0$. The χ^2 in this variant of the fit is only 5 units worse than that with the released E_{u_v} parameter; changing this parameter noticeably affects the mass determination. In addition $\mu_{f,0}^2$ is varied within 1.6 GeV$^2 < \mu_{f,0}^2 < 2.2$ GeV^2. The parameterisation uncertainty is determined at each $x_{\rm Bj}$ value from the maximal differences between the PDFs resulting from the central fit and all parameterisation variations. The total uncertainty is obtained by adding the fit, model and parameterisation uncertainties in quadrature. In the following, the quoted uncertainties correspond to 68% CL. The values of the input parameters for the fit and their variations considered, to evaluate model and parameterisation uncertainties, are listed in table A.2 of the appendix.

[4] In the FFNS this scale is decoupled from the charm quark mass.

6.2 QCD fit and determination of the running heavy quark masses

In the QCD fit, the running heavy quark masses are fitted simultaneously with the PDF parameters in equation (7). The fit yields a total $\chi^2 = 1435$ for 1208 degrees of freedom. The ratio $\chi^2/\mathrm{d.o.f.} = 1.19$ is of similar size than the values obtained in the analysis of the HERA combined inclusive data [43]. The resulting PDF set is termed HERAPDF-HQMASS. The central values of the fitted parameters are listed in table A.3 of the appendix.

In figure 13, the PDFs at the scale $\mu_{\mathrm{f},0} = 1.9$ GeV^2 are presented. Also shown are the PDFs, including experimental uncertainties, obtained by a fit to the inclusive data only with the heavy quark masses fixed to $m_c(m_c) = 1.27$ GeV and $m_b(m_b) = 4.18$ GeV [54]. No significant differences between the two PDF sets are observed. Only a slight enhancement in the gluon density of HERAPDF-HQMASS compared to that determined from the inclusive data only can be observed around $x \approx 2\cdot 10^{-3}$. This corresponds to the region in x where the charm data are most precise. When used together with the full sets of inclusive HERA data, the heavy flavour data have only little influence on the shape of the PDFs determined with quark masses fixed to their expected values. Despite the more precise heavy flavour data available in the current analysis, this finding does not alter the conclusion made on this point in the HERAPDF2.0 analysis [43]. However, the smaller uncertainties of the new combination reduce the uncertainty of the charm mass determination with respect to the previous result[5].

The running heavy quark masses are determined as:

$$
\begin{aligned}
m_c(m_c) &= 1.290^{+0.046}_{-0.041}(\mathrm{exp/fit})^{+0.062}_{-0.014}(\mathrm{mod})^{+0.003}_{-0.031}(\mathrm{par})\ \mathrm{GeV},\\
m_b(m_b) &= 4.049^{+0.104}_{-0.109}(\mathrm{exp/fit})^{+0.090}_{-0.032}(\mathrm{mod})^{+0.001}_{-0.031}(\mathrm{par})\ \mathrm{GeV}.
\end{aligned}
\tag{7}
$$

The individual contributions to the uncertainties are listed in table 5. The model uncertainties, (mod), are dominated by those arising from the scale variations. In the case of the charm quark mass, the variation in α_s yields also a sizeable contribution while the other sources lead to uncertainties of typically a few MeV, both for $m_c(m_c)$ and $m_b(m_b)$. The main contribution to the parameterisation uncertainties, (par), comes from the fit variant in which the term E_{u_v} is set to zero, other contributions are negligible. Both mass values are in agreement with the corresponding PDG values [54] and the value of $m_c(m_c)$ determined here agrees well with result from the previous analysis of HERA combined charm cross sections [38].

A cross check is performed using the Monte Carlo method [70, 71]. It is based on analysing a large number of pseudo data sets called replicas. For this cross check, 500 replicas are created by taking the combined data and fluctuating the values of the reduced cross sections randomly within their statistical and systematic uncertainties taking into account correlations. All uncertainties are assumed to follow a Gaussian distribution. The central values for the fitted parameters and their uncertainties are estimated using the mean and RMS values over the replicas. The obtained heavy-quark masses and their fit uncertainties are in agreement with those quoted in equation (7).

In order to study the influence of the inclusive data on the mass determination, fits to the combined inclusive data only are also tried. In this case, the fit results are very sensitive to

[5] The previous analysis did not consider scale variations and a less flexible PDF parameterisation was used [38]. The beauty mass determination improves the previous result based on a single data set [23].

the choice of the PDF parameterisation. When using the default 14 parameters, the masses are determined to be $m_c(m_c) = 1.80^{+0.14}_{-0.13}(\text{fit})$ GeV, $m_b(m_b) = 8.45^{+2.28}_{-1.81}(\text{fit})$ GeV, where only the fit uncertainties are quoted. In the variant of the fit using the inclusive data only and the reduced parameterisation with $E_{u_v} = 0$, the central fitted values for the heavy-quark masses are: $m_c(m_c) = 1.45$ GeV, $m_b(m_b) = 4.00$ GeV. The sensitivity to the PDF parameterisation and the large fit uncertainties for a given parameterisation demonstrate that attempts to extract heavy quark masses from inclusive HERA data alone are not reasonable in this framework. The large effect on the fitted masses observed here, when setting $E_{u_v} = 0$, motivates the E_{u_v} variation in the HERAPDF-HQMASS fit.

The NLO FFNS predictions based on HERAPDF-HQMASS are compared to the combined charm and beauty cross sections in figures 14 and 15, respectively. The predictions based on the HERAPDF2.0 set are included in the figures. Only minor differences between the different predictions can be observed. This is to be expected because of the similarities of the PDFs, in particular that of the gluon. The description of the data is similar to that observed for the predictions based on the HERAPDF2.0 FF3A set.

In figure 16 the ratios of data and predictions based HERAPDF-HQMASS to the predictions based on HERAPDF2.0 FF3A are shown for charm production. The description of the data is almost identical for both calculations. The data show a steeper $x_{\rm Bj}$ dependence than expected in NLO FFNS. The partial χ^2 value of 116 for the heavy flavour data[6] (d.o.f.= 79) in the fit presented is somewhat large. It corresponds to a p-value[7] of 0.004, which is equivalent to 2.9σ. A similar behaviour can be observed already for the charm cross sections from the previous combination [38], albeit at lower significance due to the larger uncertainties.

In figure 17 the same ratios as in figure 16 are shown for beauty production. Agreement is observed between theory and beauty data within the large uncertainties of the measurements.

6.3 $\sigma_{\rm red}^{c\bar{c}}$ and $\sigma_{\rm red}^{b\bar{b}}$ as a function of the partonic x

Since in leading-order (LO) QCD heavy flavour production proceeds via boson-gluon-fusion, at least two partons, the heavy quark pair, are present in the final state. Therefore, already in LO, the x of the parton emitted from the proton is different from $x_{\rm Bj}$ measured at the lepton vertex. At LO the gluon x is given by

$$x = x_{\rm Bj} \cdot \left(1 + \frac{\hat{s}}{Q^2}\right). \tag{8}$$

It depends on kinematic DIS variables $x_{\rm Bj}$ and Q^2 and on the invariant mass $\hat{s}$ of the heavy quark pair. At higher orders, the final state contains additional partons, such that x cannot be expressed in a simple way. Independent of the order of the calculations, only an average $\langle x \rangle$ can be determined at a given $(x_{\rm Bj}, Q^2)$ point by the integrations over all contributions to the cross section in the vicinity of this phase space point. In figure 18 the ratio of the measured

[6] It is not possible to quote the charm and the beauty contribution to this χ^2 value separately because of the correlations between the combined charm and beauty measurements.

[7] The χ^2 and the p-value given here do not correspond exactly to the statistical definition of χ^2 or p-value because the data have been used in the fit to adjust theoretical uncertainties. Therefore the theory is somewhat shifted towards the measurements. However this bias is expected to be small because the predictions are mainly constrained by the much larger and more precise inclusive data sample.

reduced cross sections to the NLO FFNS predictions based on HERAPDF-HQMASS is shown as a function of $\langle x \rangle$ instead of x_{Bj}, where $\langle x \rangle$ is the geometric mean calculated with HVQDIS. While the charm measurements cover the range $0.0005 \lesssim \langle x \rangle \lesssim 0.1$ the beauty data is limited to a higher x range, $0.004 \lesssim \langle x \rangle \lesssim 0.1$, because of the large beauty quark mass. For the charm data, a deviation from the reference calculation is evident, showing a steeper slope in x in the range $0.0005 \lesssim \langle x \rangle \lesssim 0.01$, consistent with being independent of Q^2. Due to the larger experimental uncertainties, no conclusion can be drawn for the beauty data.

6.4 Increasing the impact of the charm data on the gluon density

While inclusive DIS cross sections constrain the gluon density indirectly via scaling violations, and directly only through higher order corrections, heavy flavour production probes the gluon directly already at leading order. Contributions to heavy flavour production from light flavours are small. For charm production they amount to five to eight per cent, varying only slightly with x_{Bj} or Q^2 [45]. Because of the high precision of $\sigma_{\mathrm{red}}^{c\bar{c}}$ reached in this analysis, a study is performed to enhance the impact of the charm measurement on the gluon determination in the QCD fit.

To reduce the impact of the inclusive data in the determination of the gluon density function, a series of fits is performed, varying the values of the minimum x_{Bj} for the inclusive data included in the fit in the range $2 \cdot 10^{-4} \leq x_{\mathrm{Bj,min}} \leq 0.1$. No such requirement is applied to the heavy flavour data. The $\chi^2/\mathrm{d.o.f.}$ values for the inclusive plus heavy flavour data and the partial $\chi^2/\mathrm{d.o.f.}$ for the heavy flavour data only are presented in figure 19 as a function of $x_{\mathrm{Bj,min}}$. The partial $\chi^2/\mathrm{d.o.f.}$ for the heavy flavour data improves significantly with rising $x_{\mathrm{Bj,min}}$-cut reaching a minimum at $x_{\mathrm{Bj,min}} \approx 0.04$, while the $\chi^2/\mathrm{d.o.f.}$ for the inclusive plus heavy flavour data sample is slightly larger than that obtained without cut in x_{Bj} . For further studies $x_{\mathrm{Bj,min}} = 0.01$ is chosen. The total χ^2 is 822 for 651 degrees of freedom. The partial χ^2 of the heavy flavour data improves to 98 for 79 degrees of freedom (corresponding to a p-value of 0.07 or 1.8σ). The resulting gluon density function, shown in figure 20 at the scale $\mu_{\mathrm{f},0}^2 = 1.9\ \mathrm{GeV}^2$, is significantly steeper than the gluon density function determined when including all inclusive measurements in the fit. The other parton density functions are consistent with the result of the default fit.

In figure 21, a comparison is presented of the ratios of the combined reduced charm cross section, $\sigma_{\mathrm{red}}^{c\bar{c}}$, and the cross section as calculated from the alternative fit, in which the inclusive data are subject to the cut $x_{\mathrm{Bj}} \geq 0.01$, to the reference cross sections based on HERAPDF2.0 FF3A. The predictions from HERAPDF-HQMASS are also shown. As expected, the charm cross sections fitted with the x_{Bj} cut imposed on the inclusive data rise more strongly towards small x_{Bj} and describe the data better than the other predictions. In general, the predictions from the fit with x_{Bj} cut follow nicely the charm data. A similar study for beauty is also made but no significant differences are observed.

Cross section predictions based on the three PDF sets, discussed in the previous paragraph, are calculated for inclusive DIS. In figure 22, these predictions are compared to the inclusive reduced cross sections [43] for NC e^+p DIS. The predictions based on HERAPDF2.0 FF3A and on HERAPDF-HQMASS agree with the inclusive measurement. The calculations based on the PDF set determined by requiring $x_{\mathrm{Bj}} \geq 0.01$ for the inclusive data predict significantly larger inclusive reduced cross sections at small x_{Bj}. This illustrates the tension between the inclusive data and the charm data.

This study shows that a better description of the charm data can be achieved in NLO FFNS within the framework for PDFs applied by excluding the low-x_{Bj} inclusive data in the fit. However, the calculations then fail to describe the inclusive data at low x_{Bj}. In the theoretical framework used in this analysis, it seems impossible to resolve the $\sim 3\sigma$ difference in describing simultaneously the inclusive and charm measurements from HERA, using this simple approach of changing the gluon density. The comparison of various theory predictions to the charm data in section 5 suggests that the situation is unlikely to improve at NNLO because the NNLO predictions presented provide a poorer description of the charm data than that observed at NLO. The combined inclusive analysis [43] already revealed some tensions in the theory description of the inclusive DIS data. The current analysis reveals some additional tensions in describing simultaneously the combined charm data and the combined inclusive data. However, a dedicated investigation shows, that this does not affect the result of the mass measurements beyond the quoted uncertainties.

7 Summary

Measurements of beauty and charm production cross sections in deep inelastic ep scattering by the H1 and ZEUS experiments are combined at the level of reduced cross sections, accounting for their statistical and systematic correlations. The beauty cross sections are combined for the first time. The data sets are found to be consistent and the combined data have significantly reduced uncertainties. The charm cross sections presented in this paper are significantly more precise than those previously published.

Next-to-leading and approximate next-to-next-to-leading-order QCD predictions of different schemes are compared to data. The calculations are found to be in fair agreement with the charm data. The next-to-leading-order calculations in the fixed-flavour-number scheme provide the best description of the heavy flavour data. The beauty data, which have larger experimental uncertainties, are well described by all QCD predictions.

The combined heavy flavour data together with the published combined inclusive data from HERA are subjected to a next-to-leading-order QCD analysis in the fixed-flavour-number scheme using the $\overline{\mathrm{MS}}$ running mass definition. The running heavy quark masses are determined as $m_c(m_c) = 1.290^{+0.046}_{-0.041}(\mathrm{exp/fit})^{+0.062}_{-0.014}(\mathrm{mod})^{+0.003}_{-0.031}(\mathrm{par})$ GeV for the charm quark and $m_b(m_b) = 4.049^{+0.104}_{-0.109}(\mathrm{exp/fit})^{+0.090}_{-0.032}(\mathrm{mod})^{+0.001}_{-0.031}(\mathrm{par})$ GeV for the beauty quark. The simultaneously determined parton density functions are found to agree well with HERAPDF2.0 FF3A.

The QCD analysis reveals some tensions, at the level of $\approx 3\sigma$, in describing simultaneously the inclusive and the heavy flavour HERA DIS data. The measured reduced charm cross sections show a stronger x_{Bj} dependence than obtained in the combined QCD fit of charm and inclusive data, in which the PDFs are dominated by the fit of the inclusive data. A study in which inclusive data with $x_{\mathrm{Bj}} < 0.01$ are excluded from the fit is carried out. A much better description of the charm data can be achieved this way. However, the resulting PDFs fail to describe the inclusive data in the excluded x_{Bj} region. The alternative next-to-leading-order and next-to-next-leading-order QCD calculations considered, including those with low-x resummation, are not able to provide a better description of the combined heavy flavour data.

Acknowledgements

We are grateful to the HERA machine group whose outstanding efforts have made these experiments possible. We appreciate the contributions to the construction, maintenance and operation of the H1 and ZEUS detectors of many people who are not listed as authors. We thank our funding agencies for financial support, the DESY technical staff for continuous assistance and the DESY directorate for their support and for the hospitality they extended to the non-DESY members of the collaborations. We would like to give credit to all partners contributing to the EGI computing infrastructure for their support.

References

[1] C. Adloff *et al.* [H1 Collaboration], "Inclusive D0 and D*+- production in deep inelastic e p scattering at HERA", Z.Phys **C72**, (1996) 593 [hep-ex/9607012].

[2] J. Breitweg *et al.* [ZEUS Collaboration], "D* Production in Deep Inelastic Scattering at HERA", Phys. Lett. **B407**, (1997) 402 [hep-ex/9706009].

[3] C. Adloff *et al.* [H1 Collaboration], "Measurement of D* meson cross-sections at HERA and determination of the gluon density in the proton using NLO QCD", Nucl. Phys. **B545**, (1999) 21 [hep-ex/9812023].

[4] J. Breitweg *et al.* [ZEUS Collaboration], "Measurement of $D*^{\pm}$ production and the charm contribution to F2 in deep inelastic scattering at HERA", Eur. Phys. J. **C12**, (2000) 35 [hep-ex/9908012].

[5] C. Adloff *et al.* [H1 Collaboration], "Measurement of D*+- meson production and F2(c) in deep inelastic scattering at HERA", Phys. Lett. **B528**, (2002) 199 [hep-ex/0108039].

[6] S. Chekanov *et al.* [ZEUS Collaboration], "Measurement of D*+- production in deep inelastic e+- p scattering at HERA". Phys. Rev. **D69**, (2004) 012004 [hep-ex/0308068].

[7] A. Aktas *et al.* [H1 Collaboration], "Inclusive production of D+, D0, D+(s) and D*+ mesons in deep inelastic scattering at HERA," Eur. Phys. J. **C38**, (2005) 447 [hep-ex/0408149].

[8] A. Aktas *et al.* [H1 Collaboration], "Measurement of F2($c\bar{c}$) and F2($b\bar{b}$) at high Q^2 using the H1 vertex detector at HERA", Eur. Phys. J. **C40**, (2005) 349 [hep-ex/0411046].

[9] A. Aktas *et al.* [H1 Collaboration], "Measurement of F2(c anti-c) and F2(b anti-b) at low Q**2 and x using the H1 vertex detector at HERA", Eur. Phys. J. **C45**, (2006) 23 [hep-ex/0507081].

[10] A. Aktas *et al.* [H1 Collaboration], "Production of D*+- Mesons with Dijets in Deep-Inelastic Scattering at HERA", Eur. Phys. J. **C51**, (2007) 271 [hep-ex/0701023].

[11] S. Chekanov *et al.* [ZEUS Collaboration], "Measurement of D mesons production in deep inelastic scattering at HERA", JHEP **0707**, (2007) 074 [arXiv:0704.3562].

[12] S. Chekanov *et al.* [ZEUS Collaboration], "Measurement of D+- and D0 production in deep inelastic scattering using a lifetime tag at HERA", Eur. Phys. J. **C63**, (2009) 171 [arXiv:0812.3775].

[13] S. Chekanov *et al.* [ZEUS Collaboration], "Measurement of charm and beauty production in deep inelastic ep scattering from decays into muons at HERA", Eur. Phys. J. **C65**, (2010) 65 [arXiv:0904.3487].

[14] F. D. Aaron *et al.* [H1 Collaboration], "Measurement of the Charm and Beauty Structure Functions using the H1 Vertex Detector at HERA", Eur. Phys. J. **C65**, (2010) 89 [arXiv:0907.2643].

[15] F. D. Aaron *et al.* [H1 Collaboration], "Measurement of the D*+- Meson Production Cross Section and F(2)**(c c-bar), at High Q**2, in ep Scattering at HERA," Phys. Lett. **B686**, (2010) 91 [arXiv:0911.3989].

[16] H. Abramowicz *et al.* [ZEUS Collaboration], "Measurement of beauty production in DIS and F2bb extraction at ZEUS", Eur. Phys. J. **C69**, (2010) 347 [arXiv:1005.3396].

[17] H. Abramowicz *et al.* [ZEUS Collaboration], "Measurement of D^+ and Λ_c^+ production in deep inelastic scattering at HERA", JHEP **1011**, (2010) 009 [arXiv:1007.1945].

[18] F. D. Aaron *et al.* [H1 Collaboration], "Measurement of Charm and Beauty Jets in Deep Inelastic Scattering at HERA", Eur. Phys. J. **C71**, (2011) 1509 [arXiv:1008.1731].

[19] H. Abramowicz *et al.* [ZEUS Collaboration], "Measurement of beauty production in deep inelastic scattering at HERA using decays into electrons", Eur. Phys. J. **C71**, (2011) 1573 [arXiv:1101.3692].

[20] F. D. Aaron *et al.* [H1 Collaboration], Eur. Phys. J. **C71**, (2011) 1769 [arXiv:1106.1028].

[21] H. Abramowicz *et al.* [ZEUS Collaboration], "Measurement of $D^{\pm}$ Production in Deep Inelastic ep Scattering with the ZEUS detector at HERA", JHEP **05**, (2013) 023 [arXiv:1302.5058].

[22] H. Abramowicz *et al.* [ZEUS Collaboration], "Measurement of $D^{*\pm}$ Production in Deep Inelastic Scattering at HERA", JHEP **05**, (2013) 097 [arXiv:1303.6578]. Erratum-ibid JHEP **02**, (2014) 106.

[23] H. Abramowicz *et al.* [ZEUS Collaboration], "Measurement of beauty and charm production in deep inelastic scattering at HERA and measurement of the beauty-quark mass", JHEP **09**, (2014) 127 [arXiv:1405.6915].

[24] O. Behnke, A. Geiser and M. Lisovyi, "Charm, beauty and top at HERA", Prog. Nucl. Part. Phys. **84**, (2015) 1.

[25] E. Laenen *et al.*, "On the heavy quark content of the nucleon", Phys. Lett. **B291**, (1992) 325;
E. Laenen *et al.*, "Complete O (alpha-s) corrections to heavy flavor structure functions in electroproduction", Nucl. Phys. **B392**, (1993) 162; Nucl. Phys. B**392** (1993) 162, 229;

E. Laenen *et al.*, "O(alpha-s) corrections to heavy flavor inclusive distributions in electroproduction", Nucl. Phys. **B392**, (1993) 229;
S. Riemersma, J. Smith and W. L. van Neerven, "Rates for inclusive deep inelastic electroproduction of charm quarks at HERA", Phys. Lett. **B347**, (1995) 143 [hep-ph/9411431].

[26] S. Alekhin *et al.*, Phys. Rev. **D81**, (2010) 014032 [arXiv:0908.2766];

[27] S. Alekhin and S. Moch, arXiv:1107.0469.

[28] S. Alekhin, J. Blumlein and S. Moch, "Parton Distribution Functions and Benchmark Cross Sections at NNLO", Phys. Rev. **D86**, (2012) 054009 [arXiv:1202.2281].

[29] S. Alekhin, J. Blümlein, S. Moch and R. Placakyte, "Parton Distribution Functions, α_s and Heavy-Quark Masses for LHC Run II", Phys. Rev. **D96**, (2017) 014011 [arXiv:1701.05838].

[30] M. Glück *et al.*, Phys. Lett. **B664**, (2008) 133 [arXiv:0801.3618].

[31] H. L. Lai *et al.*, Phys. Rev. **D82**, (2010) 074024 [arXiv:1007.2241].

[32] A. D. Martin *et al.*, Eur. Phys. J. **C70**, (2010) 51 [arXiv:1007.2624].

[33] S. Alekhin and S. Moch, Phys. Lett. **B699**, (2011) 345.

[34] R. S. Thorne, "The Effect of Changes of Variable Flavour Number Scheme on PDFs and Predicted Cross Sections", Phys. Rev. **D86**, (2012) 074017 [arXiv:1201.6180].

[35] S. Forte *et al.*, Nucl. Phys. **B834**, (2010) 116 [arXiv:1001.2312].

[36] R. D. Ball *et al.* [NNPDF Collaboration], Nucl. Phys. **B849**, (2011) 296 [arXiv:1101.1300];
R. D. Ball *el al.* [NNPDF Collaboration], Nucl. Phys. **B855**, (2012) 153 [arXiv:1107.2652].

[37] R.D. Ball *et al.*, " Parton distributions with small-x resummation: evidence for BFKL dynamics in HERA data", arXiv:1710.05935.

[38] H. Abramowicz *et al.* [H1 and ZEUS Collaborations], "Combination and QCD Analysis of Charm Production Cross Section Measurements in Deep-Inelastic ep Scattering at HERA", Eur. Phys. J. **C73**, (2013) 2311 [arXiv:1211.1182].

[39] A. Glazov, Proceedings of "13$^{\text{th}}$ International Workshop on Deep Inelastic Scattering", eds. W. H. Smith and S. R. Dasu, Madison, USA, 2005, AIP Conf. Proc. **792**, (2005) 237.

[40] A. Atkas *et al.* [H1 Collaboration], "Measurement of the Inclusive ep Scattering Cross Section at Low Q^2 and x at HERA", Eur. Phys. J. **C63**, (2009) 625 [arXiv:0904.0929].

[41] F. D. Aaron *et al.* [H1 and ZEUS Collaboration], "Combined Measurement and QCD Analysis of the Inclusive e+- p Scattering Cross Sections at HERA", JHEP **01**, (2010) 109 [arXiv:0911.0884].

[42] O. Zenaiev, “Charm Production and QCD Analysis at HERA and LHC”, Ph.D. Thesis, Hamburg University, 2015 [DESY-THESIS-2015-012];

O. Zenaiev, “Charm Production and QCD Analysis at HERA and LHC”, Eur. Phys. J. **C77**, (2017) 151 [arXiv:1612.02371].

[43] H. Abramowicz *et al.* [H1 and ZEUS Collaborations], “Combination of measurements of inclusive deep inelastic $e^{\pm}p$ scattering cross sections and QCD analysis of HERA data”, Eur. Phys. J. **C75**, (2015) 580 [arXiv:1506.06042].

[44] S. Alekhin, J. Blümlein and S. Moch, “The ABM parton distributions tuned to LHC data”, Phys. Rev. **D89** (2014) 054028 [arXiv:1310.3059]; and references therein.
For some of the most recent NNLO developments, see also
J. Ablinger *et al.*, Nucl. Phy. **B890** (2014) 48 [arXiv:1409.1135]; Nucl. Phys. **B882** (2014) 263 [arXiv:1402.0359]; A. Behring *et al.*, Phys. Rev. **D92** (2015) 114005 [arXiv:1508.01449];
A. Behring *et al.*, Eur. Phys. J. **C74** (2014) 3033 [arXiv:1403.6356].

[45] K. Daum *et al.*, Proceedings of the workshop on ”Future physics at HERA”, eds. G. Ingelmann, A. De Roeck and R. Klanner, DESY, Hamburg (1996) 89 [hep-ph/9609478].

[46] B. W. Harris and J. Smith, “Charm quark and D*+- cross-sections in deeply inelastic scattering at HERA”, Phys. Rev. **D57**, (1998) 2806 [hep-ph/9706334].

[47] S. Alekhin, J. Blümlein and S. Moch, “Parton Distribution Functions and Benchmark Cross Sections at NNLO”, Phys. Rev. D86 (2012) 054009, doi: 10.1103/PhysRevD.86.054009, [arXiv:1202.2281];

I. Bierenbaum, J. Blümlein and S. Klein, “The Gluonic Operator Matrix Elements at O(alpha(s)**2) for DIS Heavy Flavor Production”, Phys. Lett. B672 (2009) 401, doi: 10.1016/j.physletb.2009.01.057, [arXiv:0901.0669];

S. Alekhin, OPENQCDRAD-1.5. `http://www-zeuthen.desy.de/~alekhin/OPENQCDRAD`.

[48] S. Alekhin *et al.*, “HERAFitter”, Eur. Phys. J. **C75**, (2015) 304 [arXiv:1410.4412], `www.xfitter.org`.

[49] I. Abt *et al.* [H1 Collaboration], Nucl. Instrum. Meth. **A386**, (1997) 310;
I. Abt *et al.* [H1 Collaboration], Nucl. Instrum. Meth. **A386**, (1997) 348;
R. D. Appuhn *et al.* [H1 SPACAL Group], Nucl. Instrum. Meth. **A386**, (1997) 397.

[50] U. Holm (ed.) [ZEUS Collaboration], “The ZEUS Detector”. Status Report (unpublished), DESY (1993), available on `http://www-zeus.desy.de/bluebook/bluebook.html`

[51] D. Pitzl *et al.*, Nucl. Instrum. Meth. **A454**, (2000) 334 [hep-ex/0002044].

[52] A. Polini *et al.*, Nucl. Instr. and Meth. **A581**, (2007) 656.

[53] A. Kwiatkowski, H. Spiesberger and H. J. Mohring, HERACLES V4.6, Comp. Phys. Commun. **69**, (1992) 155.

[54] C. Patrignani *et al.* [Particle Data Group], “2016 Review of Particle Physics”, Chin. Phys. **C40**, (2016) 100001.

[55] V. G. Kartvelishvili, A. K. Likhoded and V. A. Petrov, Phys. Lett. **B78**, (1978) 615.

[56] F. D. Aaron *et al.* [H1 Collaboration], “Study of Charm Fragmentation into $D^{*\pm}$ Mesons in Deep-Inelastic Scattering at HERA”, Eur. Phys. J. **C59**, (2009) 589 [arXiv:0808.1003].

[57] S. Chekanov *et al.* [ZEUS Collaboration], “Measurement of the charm fragmentation function in D^* photoproduction at HERA”. JHEP **04**, (2009) 082 [arXiv:0901.1210].

[58] C. Peterson *et al.*, “Scaling Violations in Inclusive e+ e- Annihilation Spectra”, Phys. Rev. **D27**, (1983) 105.

[59] P. Nason and C. Oleari, “A Phenomenological study of heavy quark fragmentation functions in e^+e^- annihilation”, Nucl. Phys. **B565**, (2000) 245 [hep-ph/9903541].

[60] M. Lisovyi *et al.*, “Combined analysis of charm-quark fragmentation-fraction measurements”, Eur. Phys. J. **C76**, (2016) 397 [arXiv:1509.01061].

[61] N. E. Adam *et al.* [Cleo Collaboration], “Absolute Branching Fraction Measurements for D+ and D0 Inclusive Semileptonic Decays”, Phys. Rev. Lett. **97**, (2006) 251801 [hep-ex/0604044].

[62] T. Sjöstrand et al., Comp. Phys. Comm. 135, 238 (2001), [hep-ph/0010017].

[63] K. Abe et al. [BELLE Collaboration], Phys. Lett. **B547**, (2002) 181, [hep-ex/0208033]; B. Aubert et al. [BABAR Collaboration], Phys. Rev. **D67**, (2003) 031101, [hep-ex/0208018].

[64] The combine data together with the full correlation information is provided at the URL `http://www.desy.de/h1zeus`

[65] V. Bertone and J. Rojo, private communication.

[66] Y. L. Dokshitzer, “Calculation of the Structure Functions for Deep Inelastic Scattering and e+ e- Annihilation by Perturbation Theory in Quantum Chromodynamics”,, Sov. Phys. JETP **46** (1977) 641 [Zh. Eksp. Teor. Fiz. **73** (1977) 1216];

V. N. Gribov and L. N. Lipatov, “Deep inelastic ep scattering in perturbation theory”, Sov. J. Nucl. Phys. 15 (1972) 438;

G. Altarelli and G. Parisi, “Asymptotic freedom in parton language”, Nucl. Phys. B126 (1977) 298, doi:10.1016/0550-3213(77)90384-4;

G. Curci, W. Furmanski and R. Petronzio, “Evolution of parton densities beyond leading order: The non-singlet case”, Nucl. Phys. B175 (1980) 27, doi:10.1016/0550-3213(80)90003-6;

W. Furmanski and R. Petronzio, “Singlet parton densities beyond leading order”, Phys. Lett. B97 (1980) 437, doi:10.1016/0370-2693(80)90636-X;

S. Moch, J. A. M. Vermaseren and A. Vogt, “The three-loop splitting functions in QCD: the non-singlet case”, Nucl. Phys. B688 (2004) 101, doi:10.1016/j.nuclphysb.2004.03.030, [arXiv:hep-ph/0403192];

A. Vogt, S. Moch and J. A. M. Vermaseren, “The three-loop splitting functions in QCD: the singlet case”, Nucl. Phys. B691 (2004) 129, doi:1 0.1016/j.nuclphysb.2004.04.024, [arXiv:hep-ph/0404111].

[67] M. Botje, “QCDNUM: Fast QCD Evolution and Convolution”, Comput. Phys. Commun. 182 (2011) 490, doi:10.1016/j.cpc.2010.10.020, [arXiv:1005.1481].

[68] F. D. Aaron *et al*. [H1 Collaboration], “Inclusive Deep Inelastic Scattering at High Q^2 with Longitudinally Polarised Lepton Beams at HERA”, JHEP **09**, (2012) 061 doi:10.1007/JHEP09(2012)061 [arXiv:1206.7007 [hep-ex]].

[69] W. J. Stirling, R. S. Thorne and G. Watt, “Parton distributions for the LHC”, Eur. Phys. J C63 (2009) 189, doi: 10.1140/epjc/s10052-009-1072-5, [arXiv:0901.0002].

[70] W. T. Giele and S. Keller, “Implications of hadron collider observables on parton distribution function uncertainties”, Phys. Rev. D **58** (1998) 094023 doi:10.1103/PhysRevD.58.094023 [hep-ph/9803393].

[71] W. T. Giele, S. A. Keller and D. A. Kosower, “Parton distribution function uncertainties”, hep-ph/0104052.

Data set	Tagging	Q^2 range [GeV^2]	$\mathscr{L}$ [pb^{-1}]	$\sqrt{s}$ [GeV]	N_c	N_b
1 H1 VTX [14]	VTX	5 – 2000	245	318	29	12
2 H1 D^{*+} HERA-I [10]	D^{*+}	2 – 100	47	318	17	
3 H1 D^{*+} HERA-II (medium Q^2) [20]	D^{*+}	5 – 100	348	318	25	
4 H1 D^{*+} HERA-II (high Q^2) [15]	D^{*+}	100 – 1000	351	318	6	
5 ZEUS D^{*+} 96-97 [4]	D^{*+}	1 – 200	37	300	21	
6 ZEUS D^{*+} 98-00 [6]	D^{*+}	1.5 – 1000	82	318	31	
7 ZEUS D^0 2005 [12]	D^0	5 – 1000	134	318	9	
8 ZEUS μ 2005 [13]	μ	20 – 10000	126	318	8	8
9 ZEUS D^+ HERA-II [21]	D^+	5 – 1000	354	318	14	
10 ZEUS D^{*+} HERA-II [22]	D^{*+}	5 – 1000	363	318	31	
11 ZEUS VTX HERA-II [23]	VTX	5 – 1000	354	318	18	17
12 ZEUS e HERA-II [19]	e	10 – 1000	363	318		9
13 ZEUS $\mu+$jet HERA-I [16]	μ	2 – 3000	114	318		11

Table 1: Data sets used in the combination. For each dataset, the tagging method, the Q^2 range, integrated luminosity ($\mathscr{L}$), centre-of-mass energy ($\sqrt{s}$) and the numbers of charm (N_c) and beauty (N_b) measurements are given. The tagging method VTX denotes inclusive measurements based on lifetime information using a silicon vertex detector.

#	Q^2 [GeV^2]	x_{Bj}	$\sigma_{\mathrm{red}}^{c\bar{c}}$	δ_{stat} [%]	δ_{uncor} [%]	δ_{cor} [%]	δ_{tot} [%]
1	2.5	0.00003	0.1142	8.9	10.7	9.4	16.9
2	2.5	0.00007	0.1105	5.8	6.7	8.2	12.1
3	2.5	0.00013	0.0911	7.1	6.2	7.9	12.3
4	2.5	0.00018	0.0917	4.8	9.6	7.2	12.9
5	2.5	0.00035	0.0544	5.3	8.2	6.9	12.0
6	5.0	0.00007	0.1532	11.6	9.6	8.2	17.1
7	5.0	0.00018	0.1539	5.3	3.4	7.8	10.0
8	5.0	0.00035	0.1164	5.2	5.3	5.7	9.3
9	5.0	0.00100	0.0776	4.8	8.7	5.6	11.4
10	7.0	0.00013	0.2249	4.3	3.3	6.7	8.6
11	7.0	0.00018	0.2023	6.8	5.7	7.2	11.4
12	7.0	0.00030	0.1767	2.3	2.4	5.4	6.4
13	7.0	0.00050	0.1616	2.5	1.8	5.2	6.0
14	7.0	0.00080	0.1199	4.6	4.0	4.9	7.8
15	7.0	0.00160	0.0902	4.1	3.9	5.2	7.7
16	12.0	0.00022	0.3161	4.9	2.9	5.7	8.0
17	12.0	0.00032	0.2904	2.9	1.5	6.3	7.1
18	12.0	0.00050	0.2410	2.4	1.3	4.6	5.3
19	12.0	0.00080	0.1813	2.1	1.4	4.5	5.1
20	12.0	0.00150	0.1476	3.2	1.5	5.1	6.2
21	12.0	0.00300	0.1010	4.4	4.0	5.1	7.8
22	18.0	0.00035	0.3198	5.2	3.3	5.2	8.1
23	18.0	0.00050	0.2905	2.6	1.4	6.4	7.0
24	18.0	0.00080	0.2554	2.2	1.2	4.2	4.9
25	18.0	0.00135	0.2016	2.0	1.1	4.1	4.7
26	18.0	0.00250	0.1630	1.9	1.3	4.2	4.7
27	18.0	0.00450	0.1137	5.5	4.1	5.4	8.7

Table 2: The averaged reduced cross section for charm production, $\sigma_{\mathrm{red}}^{c\bar{c}}$, obtained by the combination of H1 and ZEUS measurements. The cross section values are given together with the statistical (δ_{stat}) and the uncorrelated (δ_{uncor}) and correlated (δ_{cor}) systematic uncertainties. The total uncertainties (δ_{tot}) are obtained through adding the statistical, uncorrelated and correlated systematic uncertainties in quadrature. All uncertainties are quoted in per cent.

#	Q^2 [GeV^2]	x_{Bj}	$\sigma_{\mathrm{red}}^{c\bar{c}}$	δ_{stat}[%]	δ_{uncor}[%]	δ_{cor}[%]	δ_{tot}[%]
28	32.0	0.00060	0.3885	8.5	9.3	5.8	13.9
29	32.0	0.00080	0.3756	2.3	1.4	4.4	5.2
30	32.0	0.00140	0.2807	2.0	1.1	3.4	4.1
31	32.0	0.00240	0.2190	2.3	1.4	3.9	4.7
32	32.0	0.00320	0.2015	3.6	1.6	5.4	6.6
33	32.0	0.00550	0.1553	4.2	3.0	4.1	6.6
34	32.0	0.00800	0.0940	8.7	5.4	6.0	11.9
35	60.0	0.00140	0.3254	3.2	1.4	4.8	5.9
36	60.0	0.00200	0.3289	2.3	1.2	4.1	4.9
37	60.0	0.00320	0.2576	2.2	1.2	3.6	4.4
38	60.0	0.00500	0.1925	2.3	1.6	4.1	5.0
39	60.0	0.00800	0.1596	4.8	3.1	3.4	6.7
40	60.0	0.01500	0.0946	8.1	6.5	4.9	11.5
41	120.0	0.00200	0.3766	3.3	2.6	5.0	6.5
42	120.0	0.00320	0.2274	14.6	13.7	2.7	20.2
43	120.0	0.00550	0.2173	3.3	1.6	5.4	6.5
44	120.0	0.01000	0.1519	3.9	2.3	5.2	6.9
45	120.0	0.02500	0.0702	13.6	12.6	4.4	19.1
46	200.0	0.00500	0.2389	3.1	2.4	4.5	6.0
47	200.0	0.01300	0.1704	3.4	2.3	5.0	6.5
48	350.0	0.01000	0.2230	5.1	3.0	6.4	8.7
49	350.0	0.02500	0.1065	6.1	2.9	7.4	10.0
50	650.0	0.01300	0.2026	5.4	3.7	9.1	11.2
51	650.0	0.03200	0.0885	7.8	3.8	12.8	15.4
52	2000.0	0.05000	0.0603	16.0	6.7	26.4	31.6

Table 2: continued

#	Q^2 [GeV^2]	x_{Bj}	$\sigma_{\mathrm{red}}^{b\bar{b}}$	δ_{stat}	δ_{uncor}	δ_{cor}	δ_{tot}
1	2.5	0.00013	0.0018	28.4	22.4	11.4	37.9
2	5.0	0.00018	0.0048	10.5	7.1	19.8	23.5
3	7.0	0.00013	0.0059	8.8	11.2	12.7	19.1
4	7.0	0.00030	0.0040	8.5	10.3	15.2	20.2
5	12.0	0.00032	0.0072	4.9	5.8	10.5	13.0
6	12.0	0.00080	0.0041	4.6	6.9	11.1	13.9
7	12.0	0.00150	0.0014	32.2	26.9	3.6	42.1
8	18.0	0.00080	0.0082	4.8	5.0	12.8	14.5
9	32.0	0.00060	0.0207	8.9	7.8	8.9	14.8
10	32.0	0.00080	0.0152	5.8	6.1	10.0	13.1
11	32.0	0.00140	0.0113	3.9	5.3	9.0	11.2
12	32.0	0.00240	0.0082	9.0	9.5	12.9	18.4
13	32.0	0.00320	0.0046	32.2	41.9	3.0	52.9
14	32.0	0.00550	0.0058	39.8	20.4	57.4	72.8
15	60.0	0.00140	0.0260	4.8	6.9	8.8	12.2
16	60.0	0.00200	0.0167	7.5	6.5	10.5	14.4
17	60.0	0.00320	0.0097	10.7	7.7	14.4	19.5
18	60.0	0.00500	0.0129	5.4	4.2	14.7	16.2
19	120.0	0.00200	0.0288	6.3	5.4	9.0	12.2
20	120.0	0.00550	0.0127	21.2	14.9	10.9	28.1
21	120.0	0.01000	0.0149	20.5	20.6	23.6	37.5
22	200.0	0.00500	0.0274	3.8	3.7	6.9	8.7
23	200.0	0.01300	0.0123	9.5	4.8	19.5	22.2
24	350.0	0.02500	0.0138	20.4	26.2	35.0	48.2
25	650.0	0.01300	0.0164	8.1	7.5	13.1	17.1
26	650.0	0.03200	0.0103	8.1	8.7	14.6	18.8
27	2000.0	0.05000	0.0052	30.6	15.2	47.6	58.6

Table 3: The averaged reduced cross section for beauty production, $\sigma_{\mathrm{red}}^{b\bar{b}}$, obtained by the combination of H1 and ZEUS measurements. The cross section values are given together with the statistical (δ_{stat}) and the uncorrelated (δ_{uncor}) and correlated (δ_{cor}) systematic uncertainties. The total uncertainties (δ_{tot}) are obtained through adding the statistical, uncorrelated and correlated systematic uncertainties in quadrature. All uncertainties are quoted in per cent.

Dataset	PDF (scheme)	χ^2 [p-value]
charm [38]	HERAPDF20_NLO_FF3A (FFNS)	59 [0.23]
	ABKM09 (FFNS)	59 [0.23]
	ABMP16_3_nlo (FFNS)	61 [0.18]
	ABMP16_3_nnlo (FFNS)	70 [0.05]
	HERAPDF20_NLO_EIG (RT OPT)	71 [0.04]
(N_{dat} = 52)	HERAPDF20_NNLO_EIG (RT OPT)	66 [0.09]
	NNPDF31sx NNLO (FONLL-C)	106 [$1.5 \cdot 10^{-6}$]
(N_{dat} = 47)	NNPDF31sx NNLO+NLLX (FONLL-C)	71 [0.013]
charm, this analysis	HERAPDF20_NLO_FF3A (FFNS)	86 [0.002]
	ABKM09 (FFNS)	82 [0.005]
	ABMP16_3_nlo (FFNS)	90 [0.0008]
	ABMP16_3_nnlo (FFNS)	109 [$6 \cdot 10^{-6}$]
	HERAPDF20_NLO_EIG (RT OPT)	99 [$9 \cdot 10^{-5}$]
(N_{dat} = 52)	HERAPDF20_NNLO_EIG (RT OPT)	102 [$4 \cdot 10^{-5}$]
	NNPDF31sx NNLO (FONLL-C)	140 [$1.5 \cdot 10^{-11}$]
(N_{dat} = 47)	NNPDF31sx NNLO+NLLX (FONLL-C)	114 [$5 \cdot 10^{-7}$]
beauty (N_{dat} = 27)	HERAPDF20_NLO_FF3A (FFNS)	33[0.20]
	ABMP16_3_nlo (FFNS)	37 [0.10]
	ABMP16_3_nnlo (FFNS)	41 [0.04]
	HERAPDF20_NLO_EIG (RT OPT)	33 [0.20]
	HERAPDF20_NNLO_EIG (RT OPT)	45 [0.016]

Table 4: The χ^2, p-values and number of data points of the charm and beauty data with respect to the NLO and approximate NNLO calculations using various PDFs as described in the text. The χ^2 values that include PDF uncertainties are shown separately. The measurements at $Q^2 = 2.5$ GeV^2 are excluded in the calculations of the χ^2 values for the NNPDF3.1sx predictions, by which the number of data points is reduced to 47. (See caption of figure 12 for further explantions.)

Parameter	Variation	$m_c(m_c)$ uncertainty (GeV)	$m_b(m_b)$ uncertainty (GeV)
Experimental / Fit uncertainty			
Total	$\Delta\chi^2 = 1$	$^{+0.046}_{-0.041}$	$^{+0.104}_{-0.109}$
Model uncertainty			
f_s	$0.4^{+0.1}_{-0.1}$	$^{-0.003}_{+0.004}$	$^{-0.001}_{+0.001}$
$Q^2_{\rm min}$	$3.5^{+1.5}_{-1.0}$ GeV^2	$^{-0.001}_{+0.007}$	$^{-0.005}_{+0.007}$
$\mu_{r,f}$	$\mu_{r,f}{}^{\times 2.0}_{\times 0.5}$	$^{+0.030}_{+0.060}$	$^{-0.032}_{+0.090}$
$\alpha_s^{n_f=3}(M_Z)$	$0.106^{+0.0015}_{-0.0015}$	$^{-0.014}_{+0.011}$	$^{+0.002}_{-0.005}$
Total		$^{+0.062}_{-0.014}$	$^{+0.090}_{-0.032}$
PDF parameterisation uncertainty			
$\mu^2_{\rm f,0}$	1.9 ± 0.3 GeV^2	$^{+0.003}_{-0.001}$	$^{-0.001}_{+0.001}$
E_{u_v}	set to 0	-0.031	-0.031
Total		$^{+0.003}_{-0.031}$	$^{+0.001}_{-0.031}$

Table 5: List of uncertainties for the charm and beauty quark mass determination. The rest of PDF parameterisation uncertainties have no effect on $m_c(m_c)$ and $m_b(m_b)$.

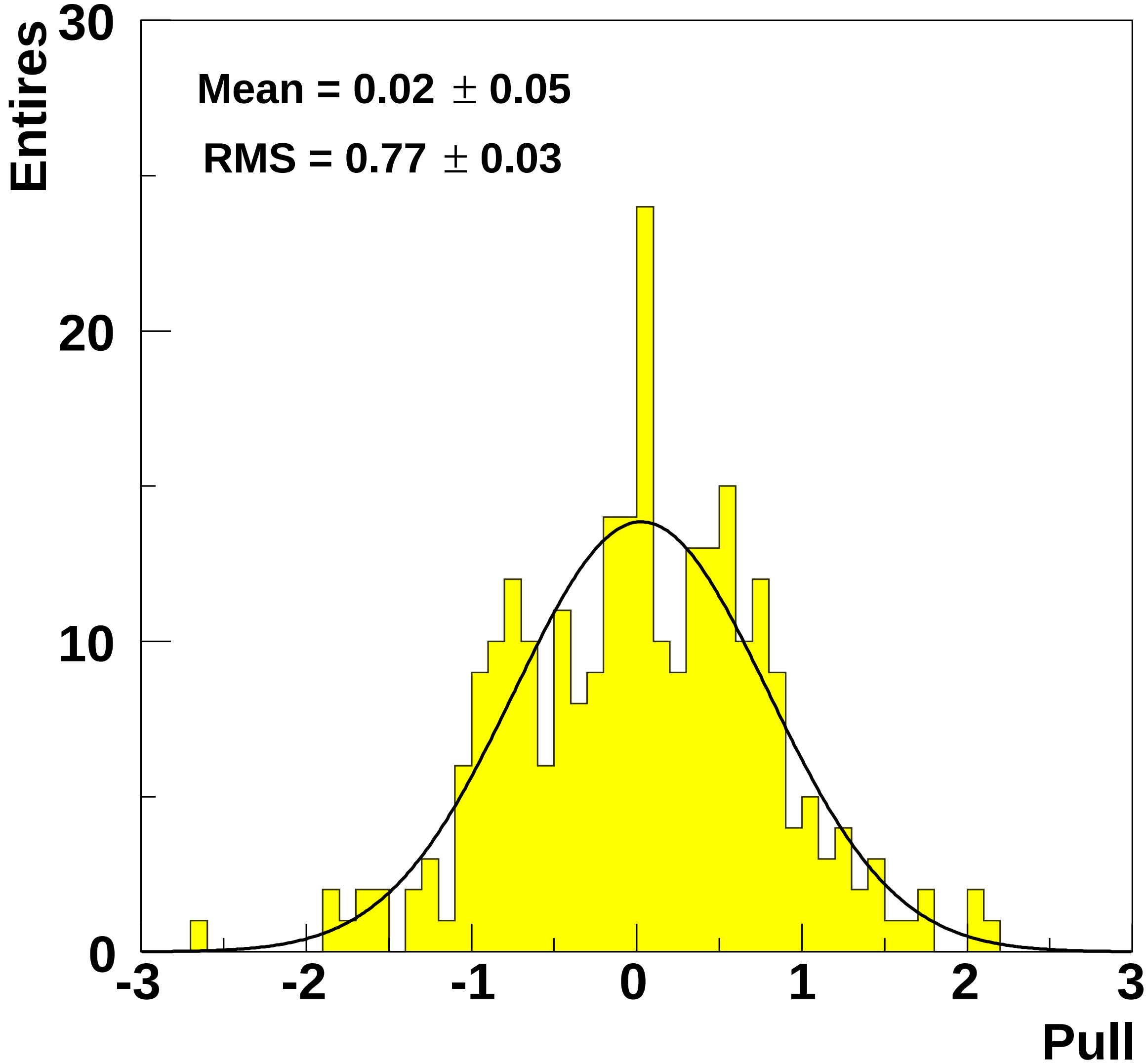

Figure 1: The pull distribution for the combination of the charm and beauty reduced cross sections (shaded histogram). The solid line shows a fit of a Gaussian to the pull distribution. The mean and RMS values given are the results from the fit.

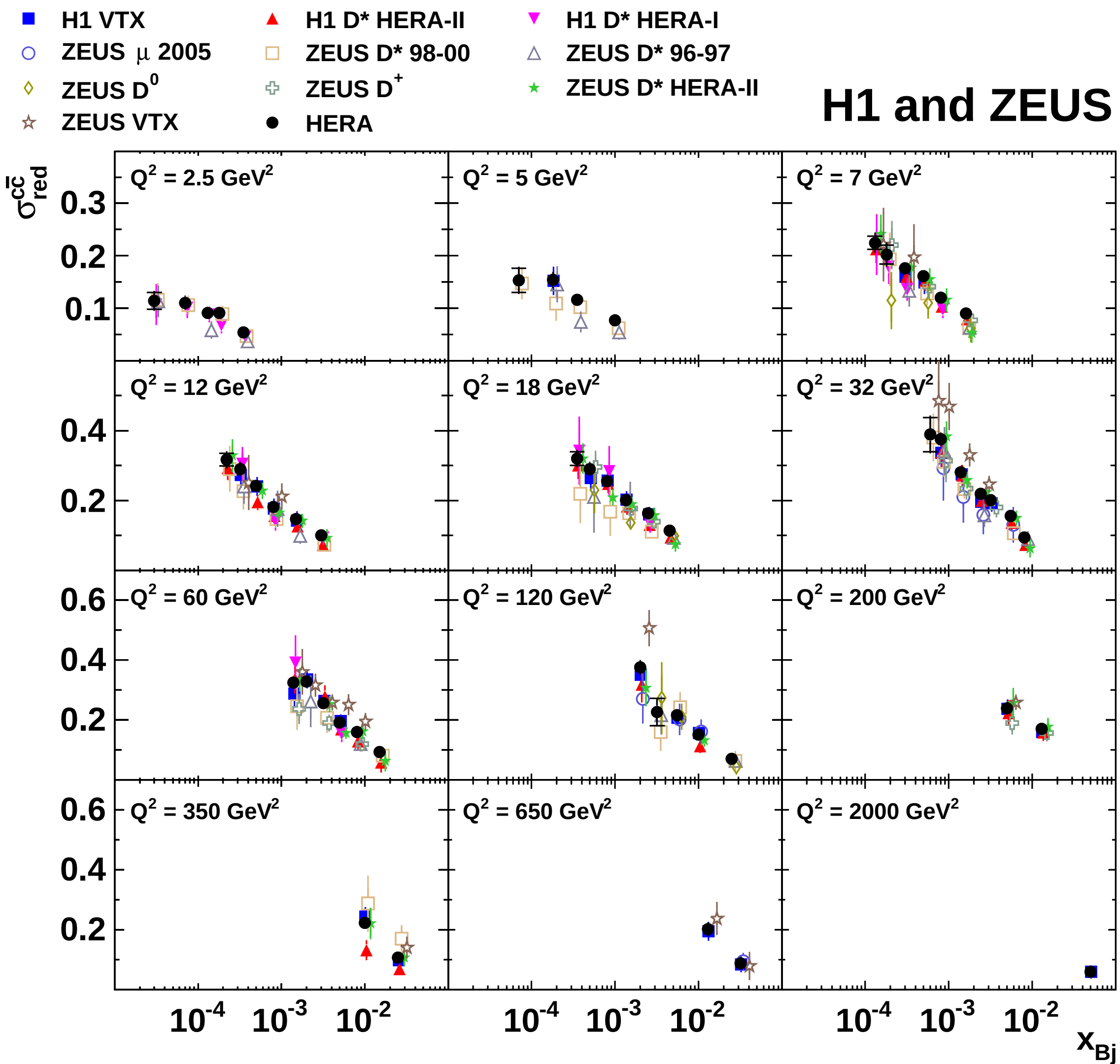

Figure 2: Combined measurements of the reduced charm production cross sections, $\sigma_{\rm red}^{c\bar{c}}$, (full circles) as a function of $x_{\rm Bj}$ for different values of Q^2. The inner error bars indicate the uncorrelated part of the uncertainties and the outer error bars represent the total uncertainties. The input measurements are also shown by the different markers. For presentation purposes each individual measurement is shifted in $x_{\rm Bj}$.

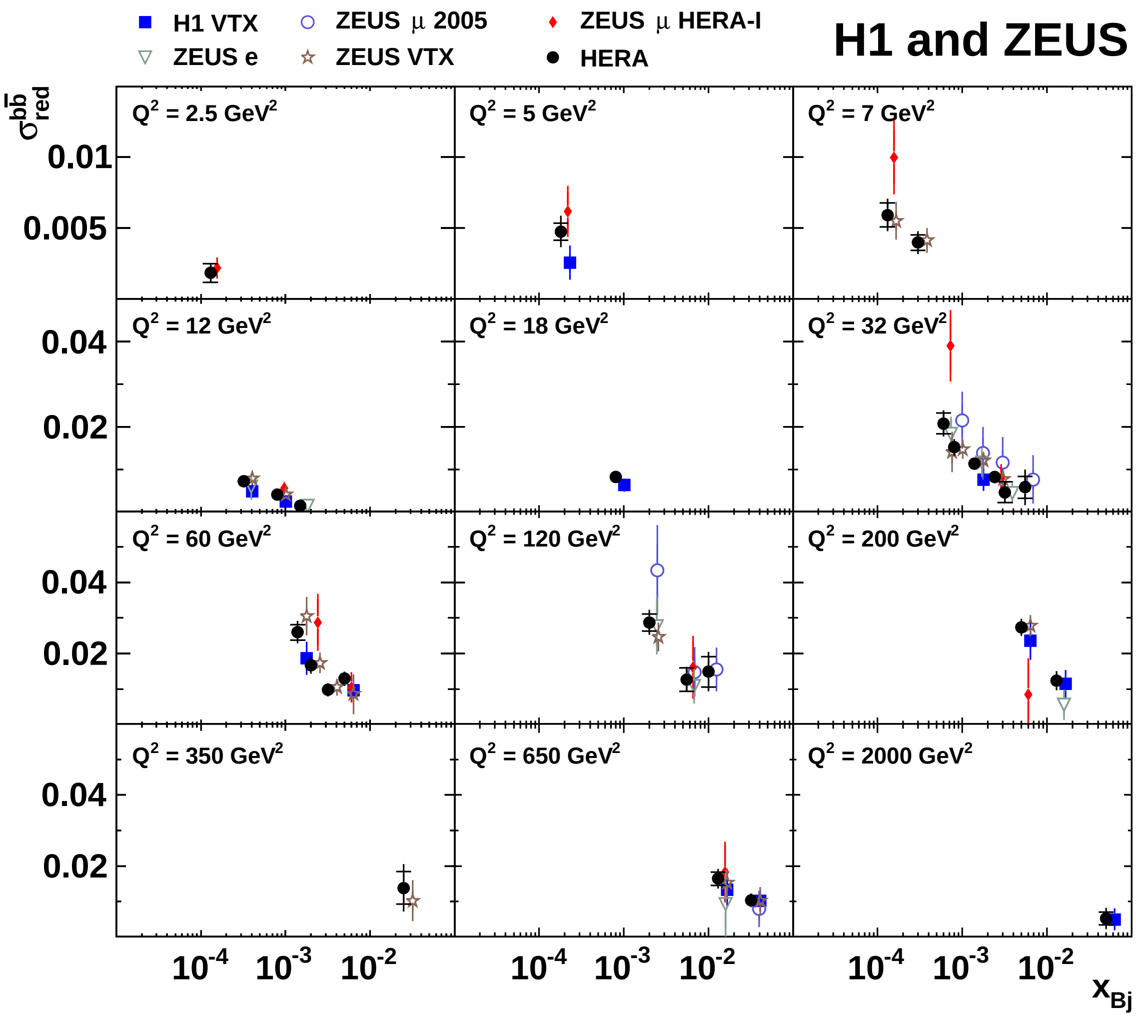

Figure 3: Combined measurements of the reduced beauty production cross sections, $\sigma_{\rm red}^{b\bar{b}}$, (full circles) as a function of $x_{\rm Bj}$ for different values of Q^2. The inner error bars indicate the uncorrelated part of the uncertainties and the outer error bars represent the total uncertainties. The input measurements are also shown by the different markers. For presentation purposes each individual measurement is shifted in $x_{\rm Bj}$.

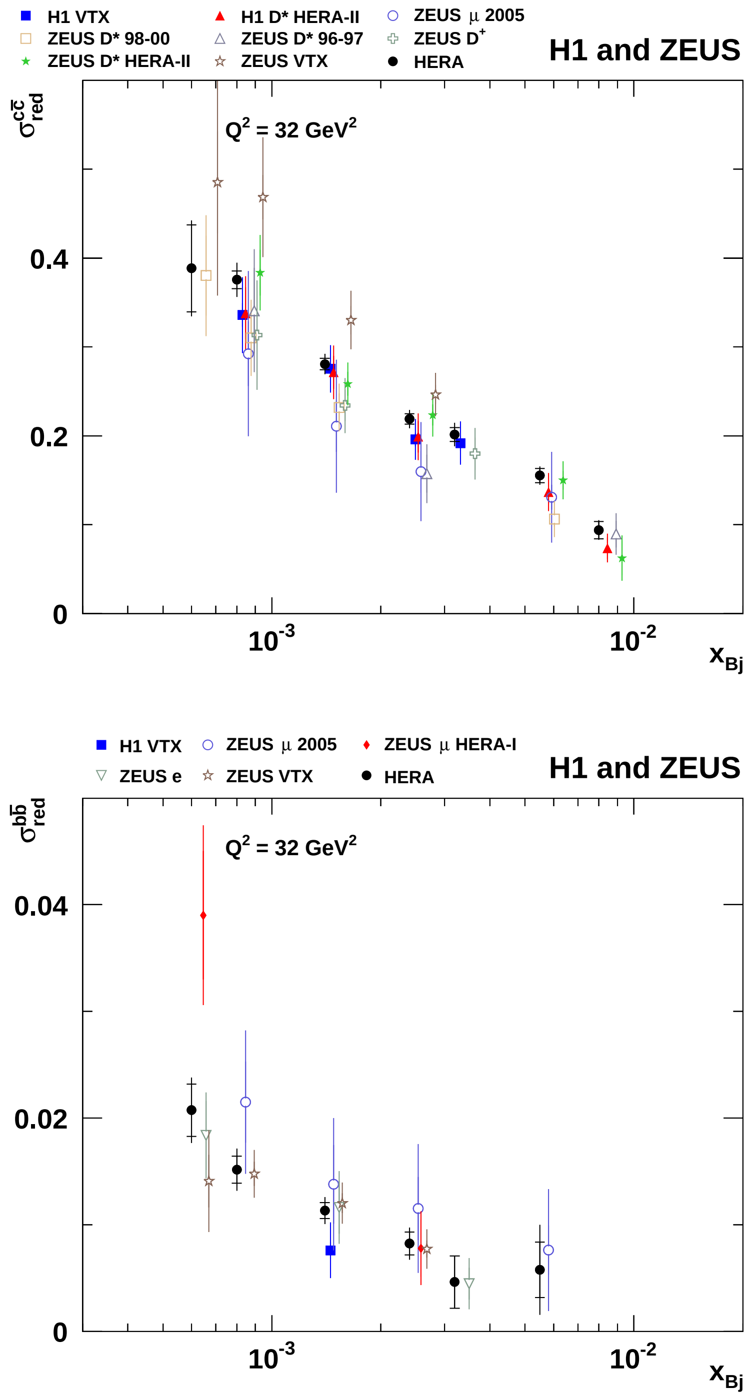

Figure 4: Reduced cross sections as a function of x_{Bj} at $Q^2 = 32$ GeV^2 for charm (upper panel) and beauty production (lower panel). The combined cross sections (full black circles) are compared to the input measurements shown by the different markers. The inner error bars indicate the uncorrelated part of the uncertainties and the outer error bars represent the total uncertainties. For better visibility the individual input data are slightly displaced in x_{Bj} towards larger values.

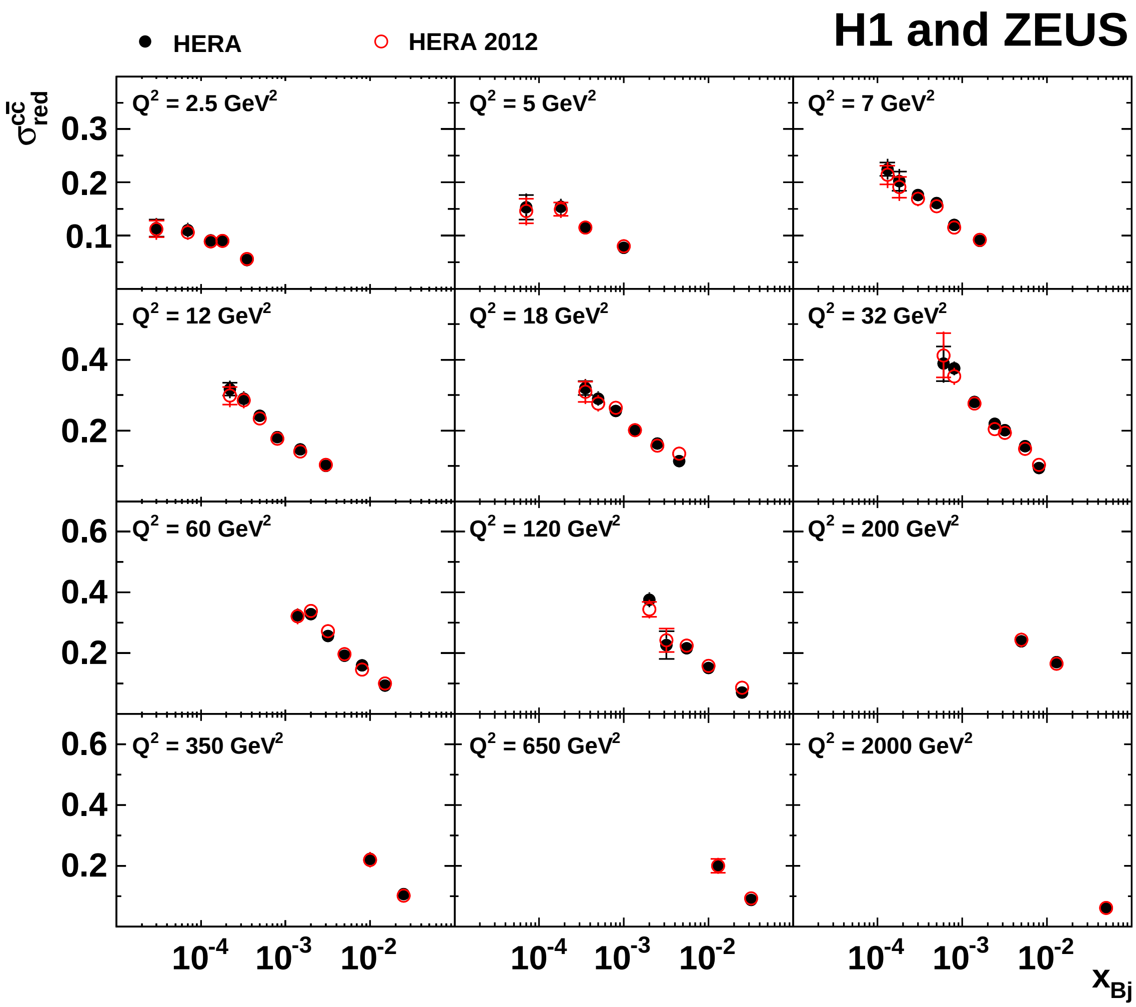

Figure 5: Combined reduced cross sections, $\sigma_{\rm red}^{c\bar{c}}$, (full circles) as a function of $x_{\rm Bj}$ for given values of Q^2, compared to the results of the previous combination [38], denoted as 'HERA 2012' (open circles).

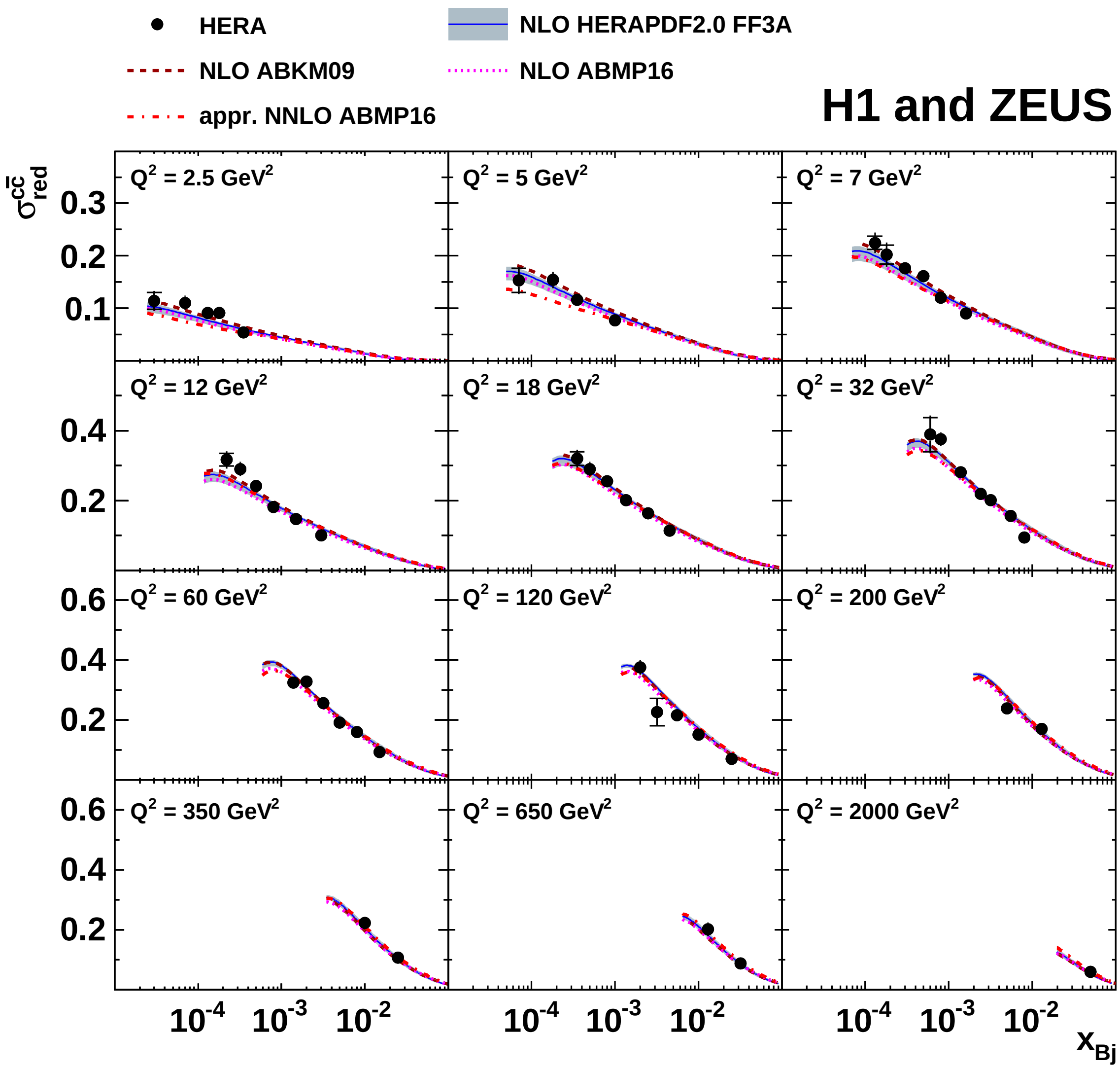

Figure 6: Combined reduced charm cross sections, $\sigma_{\rm red}^{c\bar{c}}$, (full circles) as a function of $x_{\rm Bj}$ for given values of Q^2, compared to the NLO QCD FFNS predictions based on the HERAPDF2.0 FF3A (solid lines), ABKM09 (dashed lines) and ABMP16 (dotted lines) PDF sets. Also shown is the approximate NNLO prediction using ABMP16 (dashed-dotted lines). The shaded bands on the HERAPDF2.0 FF3A predictions show the theory uncertainties obtained by adding PDF, scale and charm quark mass uncertainties in quadrature.

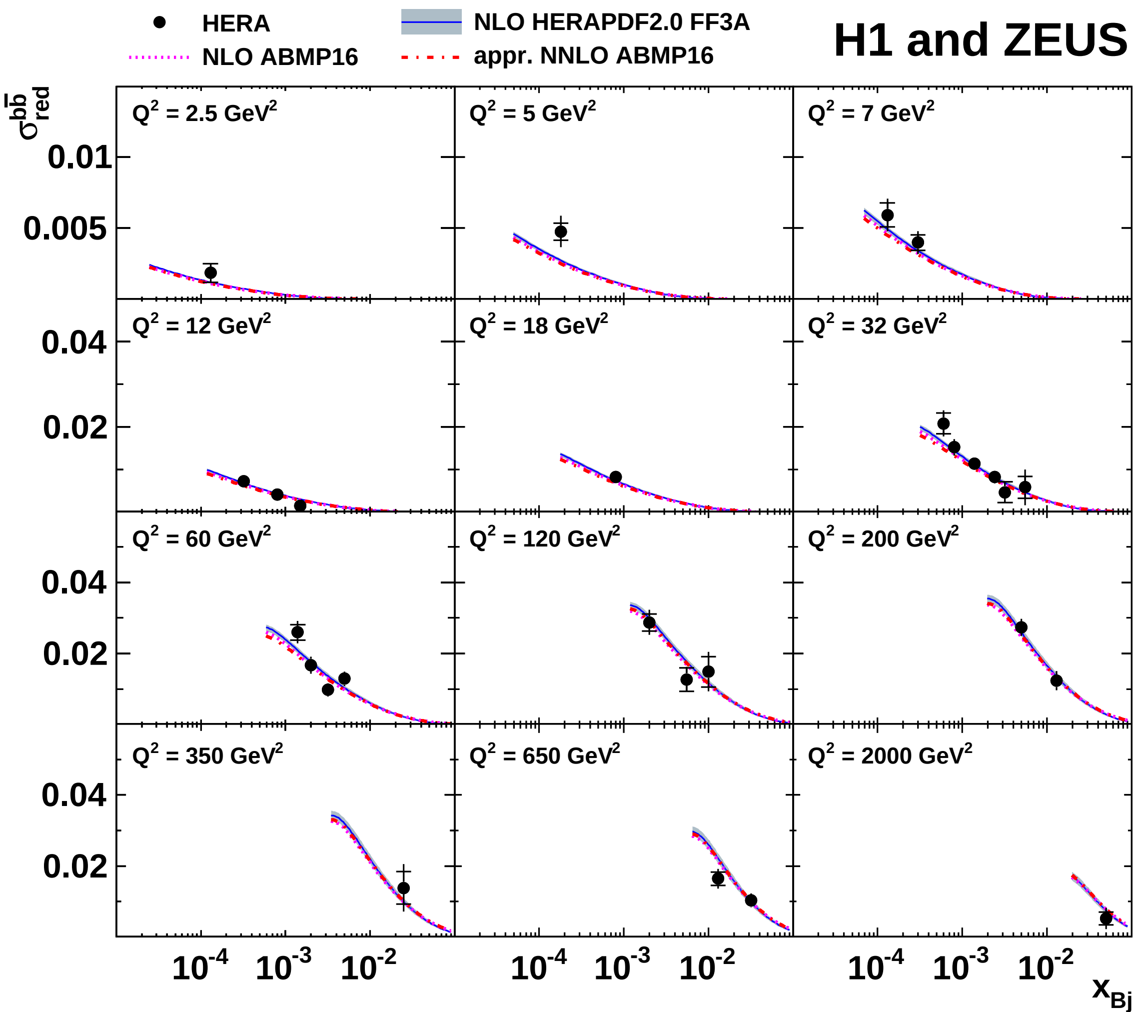

Figure 7: Combined reduced beauty cross sections, $\sigma_{\rm red}^{b\bar{b}}$, (full circles) as a function of $x_{\rm Bj}$ for given values of Q^2, compared to the NLO QCD FFNS predictions based on the HERAPDF2.0 FF3A (solid lines), ABKM09 (dashed lines) and ABMP16 (dotted lines) PDF sets. Also shown is the prediction in approximate NNLO using ABMP16 (dashed-dotted lines). The shaded bands on the HERAPDF2.0 FF3A predictions show the theory uncertainties obtained by adding PDF, scale and beauty quark mass uncertainties in quadrature.

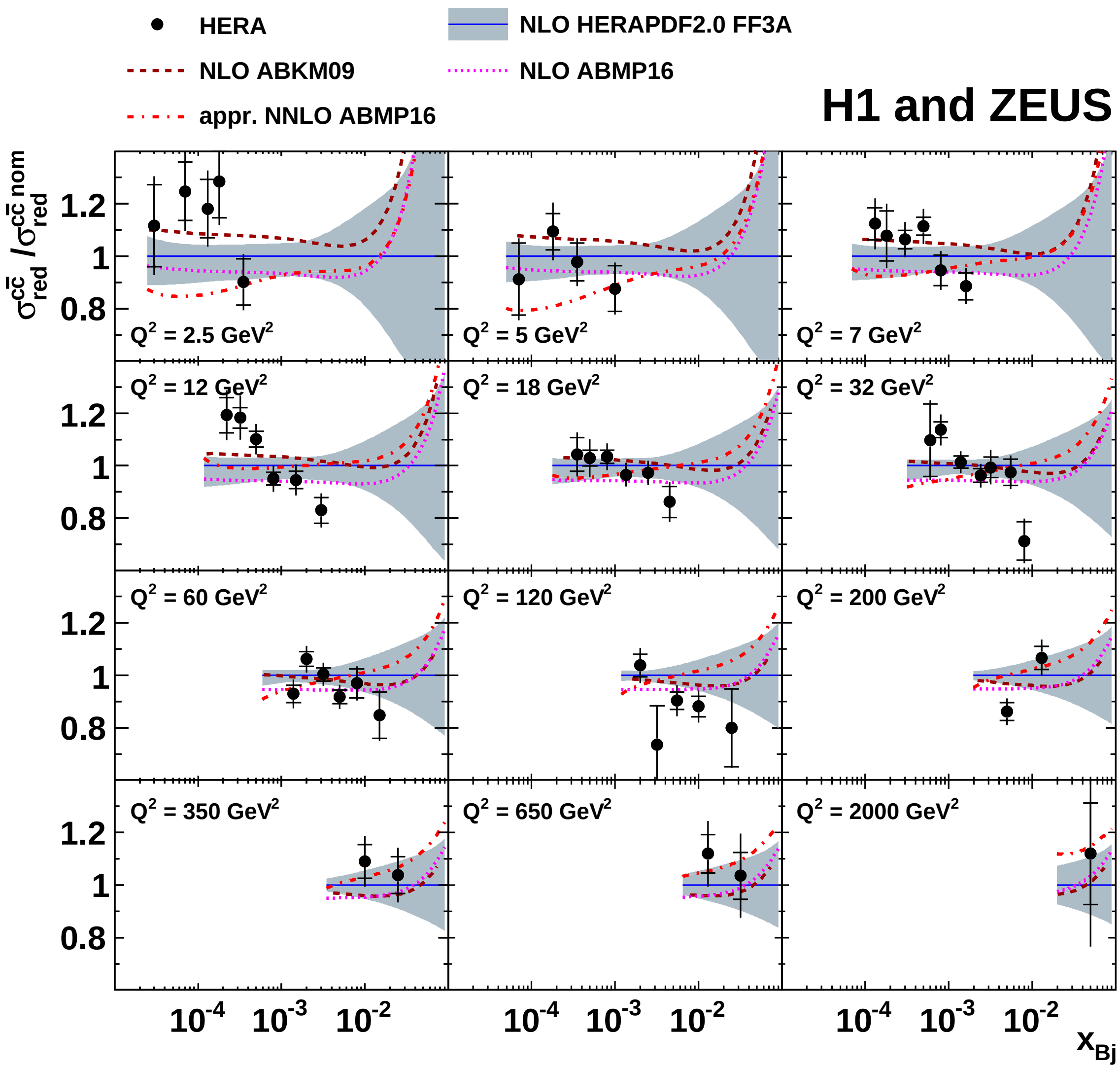

Figure 8: Combined reduced charm cross sections, $\sigma_{\rm red}^{c\bar{c}}$, (full circles) as a function of $x_{\rm Bj}$ for given values of Q^2, compared to the NLO (dashed and dotted lines) and approximate NNLO (dashed-dotted lines) QCD theoretical FFNS predictions obtained using various PDFs, as in Fig. 6, normalised to the predictions obtained using HERAPDF2.0 FF3A (solid lines with shaded uncertainty bands).

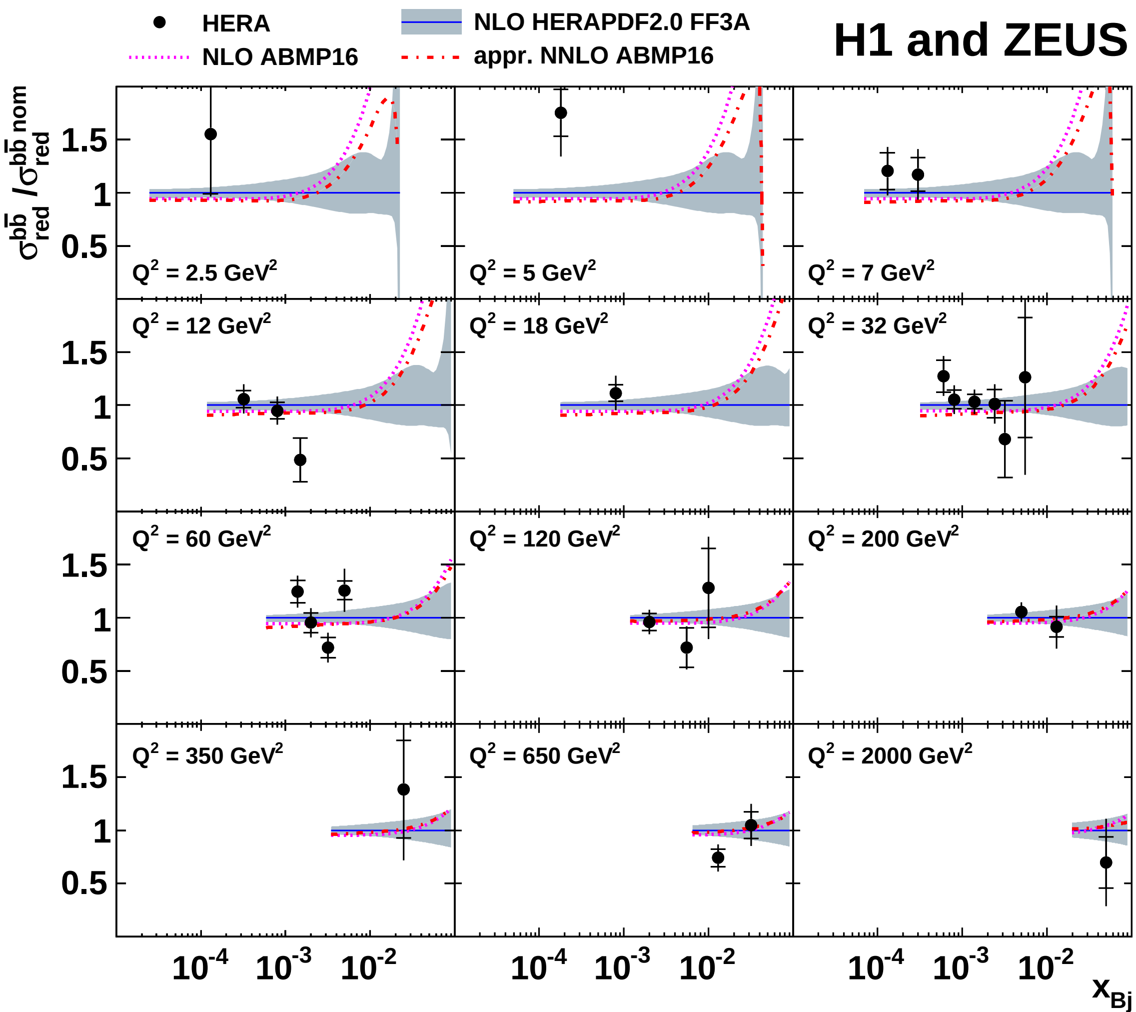

Figure 9: Combined reduced beauty cross sections, $\sigma_{\rm red}^{b\bar{b}}$, (full circles) as a function of $x_{\rm Bj}$ for given values of Q^2, compared to the NLO (dotted bands) and approximate NNLO (dashed-dotted bands) QCD theoretical FFNS predictions obtained using various PDFs, as in Fig. 7, normalised to the predictions obtained using HERAPDF2.0 FF3A (solid lines with shaded uncertainty bands).

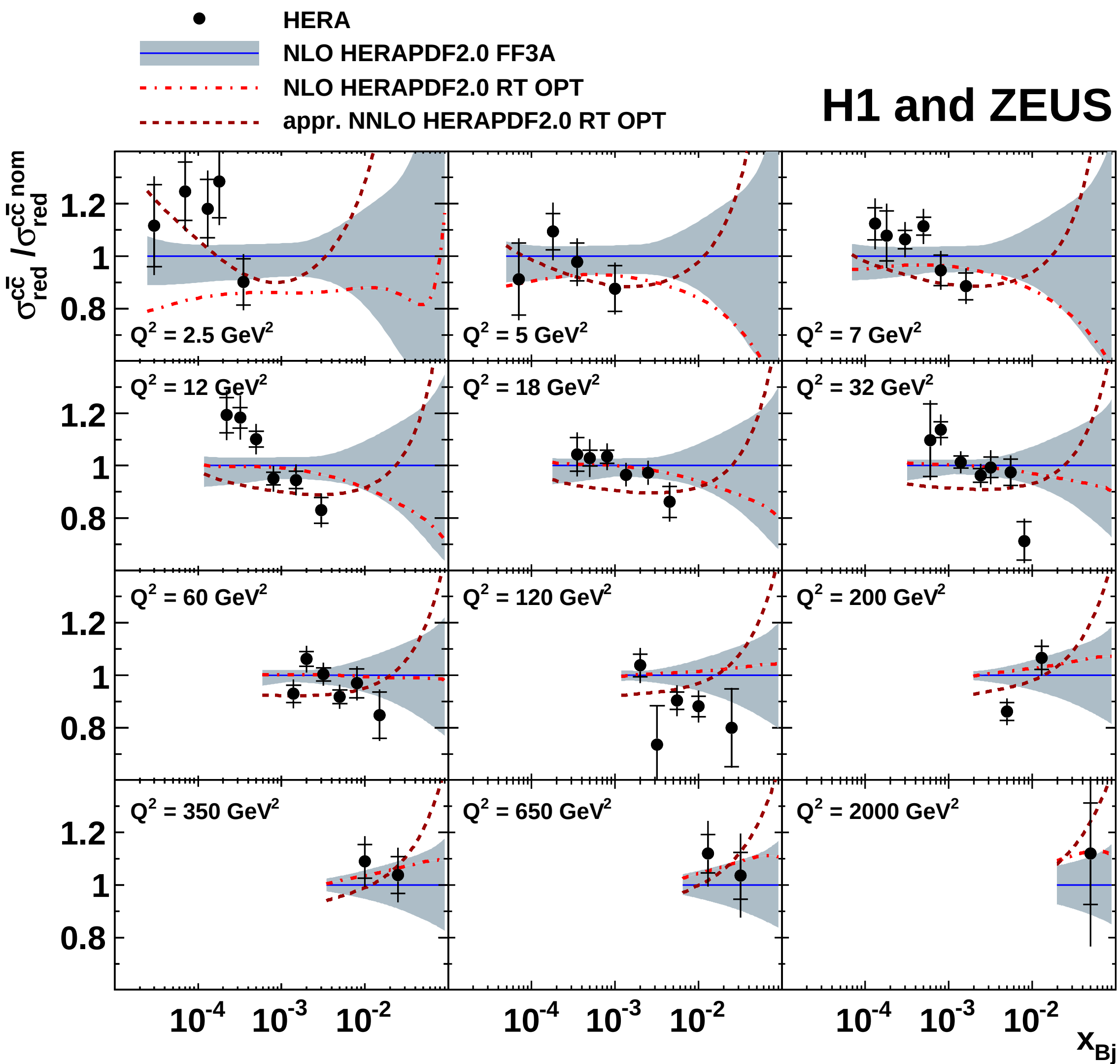

Figure 10: Combined reduced charm cross sections, $\sigma_{\rm red}^{c\bar{c}}$, (full circles) as a function of $x_{\rm Bj}$ for given values of Q^2, compared to NLO (dashed-dotted lines) and approximate NNLO (dashed lines) VFNS predictions based on HERAPDF2.0 using corresponding NLO and NNLO HERAPDF2.0 PDF sets, normalised to the FFNS predictions obtained using HERAPDF2.0 FF3A (solid lines with shaded uncertainty bands). The uncertainties for the VFNS predictions are of similar size to those presented for the FFNS calculation.

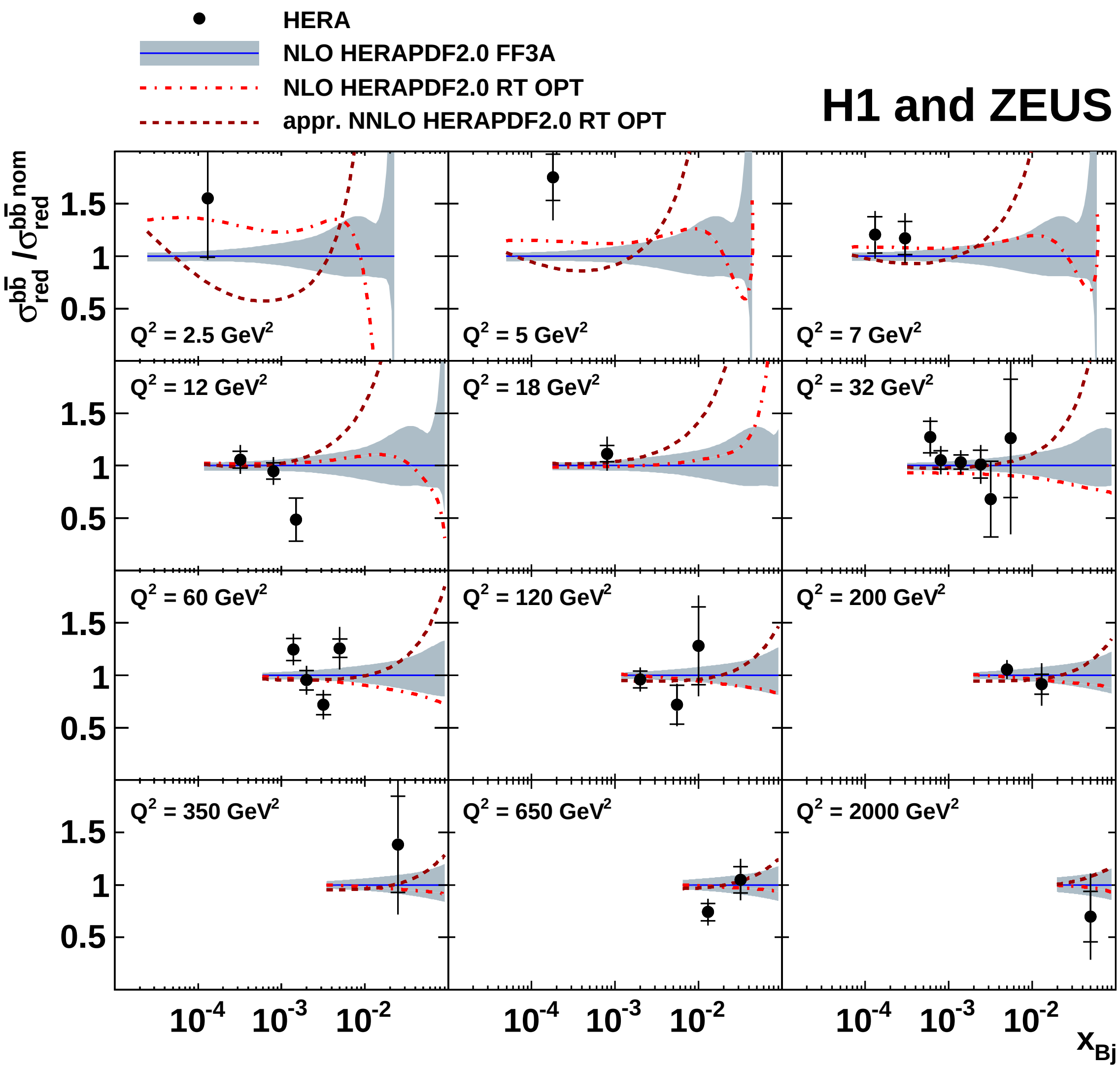

Figure 11: Combined reduced beauty cross sections, $\sigma_{\text{red}}^{b\bar{b}}$, (full circles) as a function of x_{Bj} for given values of Q^2, compared to the NLO (dashed-dotted lines) and approximate NNLO (dashed lines) VFNS predictions based on HERAPDF2.0 using corresponding NLO and NNLO HERAPDF2.0 PDF sets, normalised to the FFNS predictions obtained using HERAPDF2.0 FF3A (solid lines with shaded uncertainty bands). For the VFNS predictions no uncertainties are given. These are in size similar to those presented for the FFNS calculation.

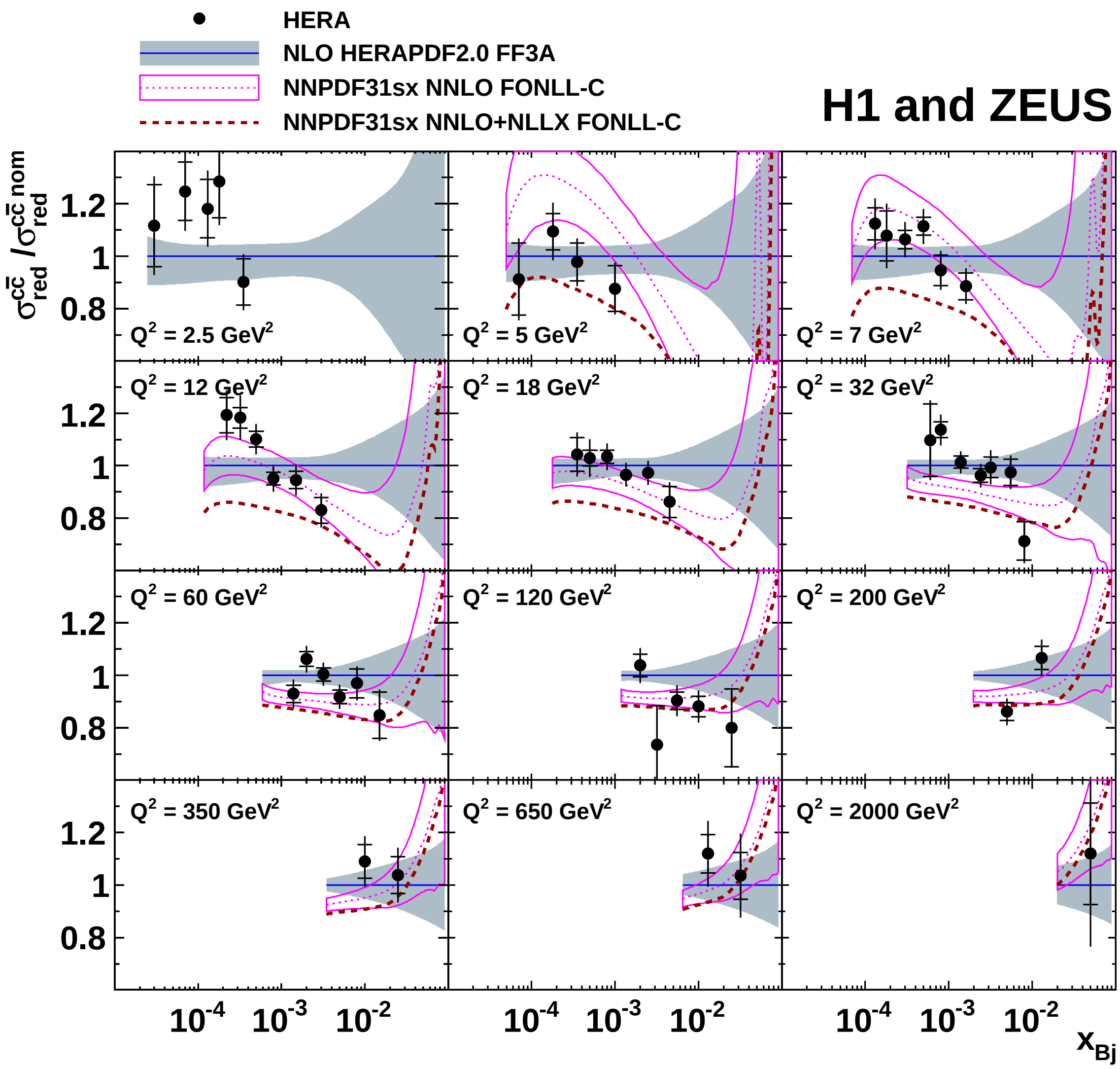

Figure 12: Combined reduced charm cross sections, $\sigma_{\rm red}^{c\bar{c}}$, (full circles) as a function of $x_{\rm Bj}$ for given values of Q^2, compared to VFNS predictions of the NNPDF group normalised to the FFNS predictions obtained using HERAPDF2.0 FF3A (solid lines with shaded uncertainty bands). Results from two different calculations are shown: without (FONNL-C, dotted lines with uncertainty bands) and with low-x resummation (FONNL-C+NLLsx , dashed lines). For the calculations the NNPDF3.1sx PDF set is used. For better clarity of the presentation the uncertainties of the FONNL+NLLsx calculations are not shown. These are in size similar to those shown for the FONLL calculations. No FONNL predictions based on NNPDF3.1sx are shown at $Q^2 = 2.5$ GeV^2 because this value lies below the starting scale of the QCD evolution in the calculation (2.6 GeV^2).

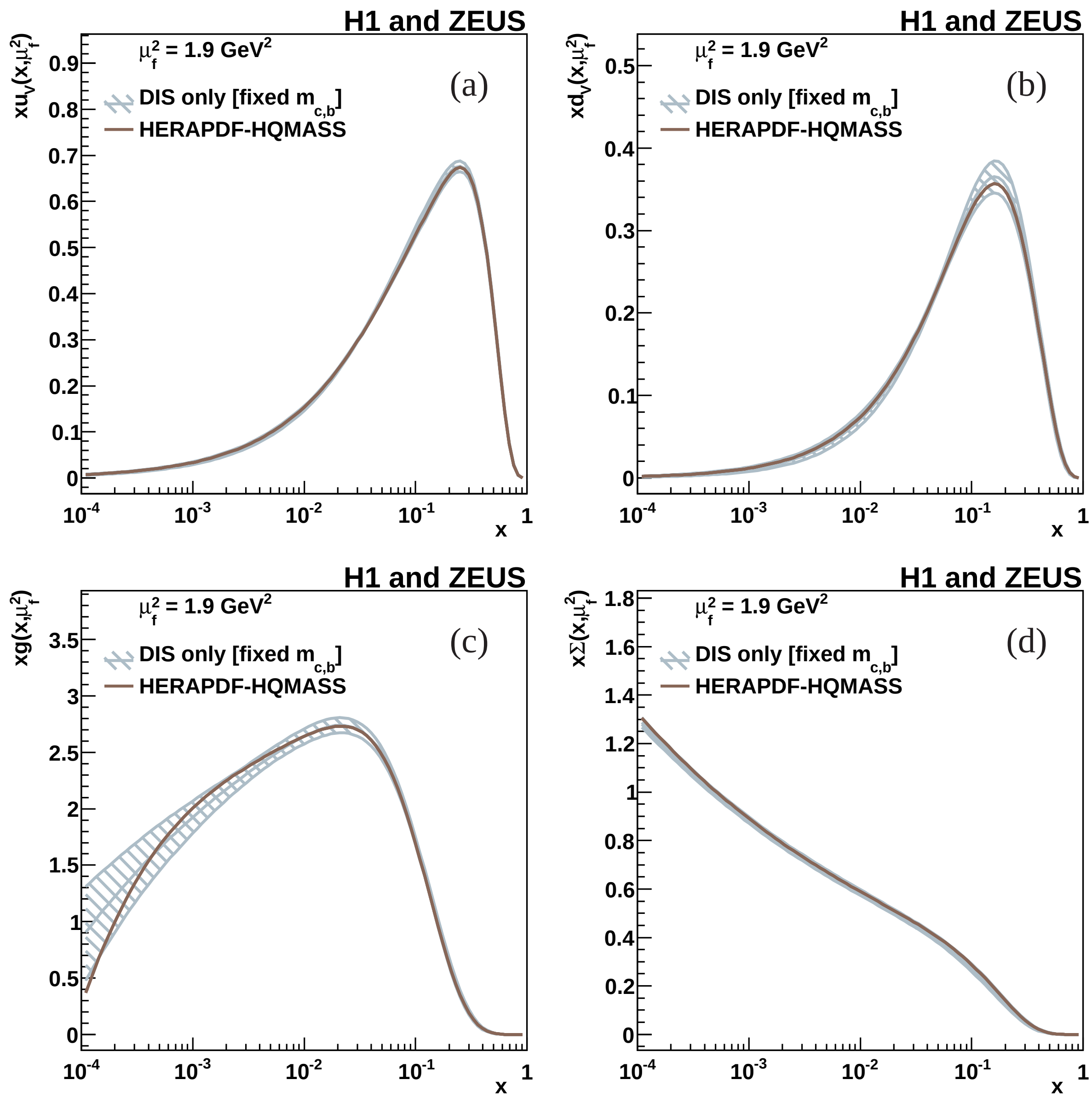

Figure 13: Parton density functions $x \cdot f(x, Q^2)$ at the starting scale $Q_0^2 = 1.9$ GeV^2 with $f = u_v, d_v, g, \Sigma$ for the valence up quark (a), the valence down quark (b), the gluon (c) and the sea quarks (d) of HERAPDF-HQMASS (solid dark lines) and obtained from a fit to the combined inclusive data only (light grey lines). The experimental/fit uncertainties obtained from the fit to the combined inclusive and heavy flavour data are indicated by the hatched bands. For better visibility only the uncertainties for the fit to the inclusive data are shown.

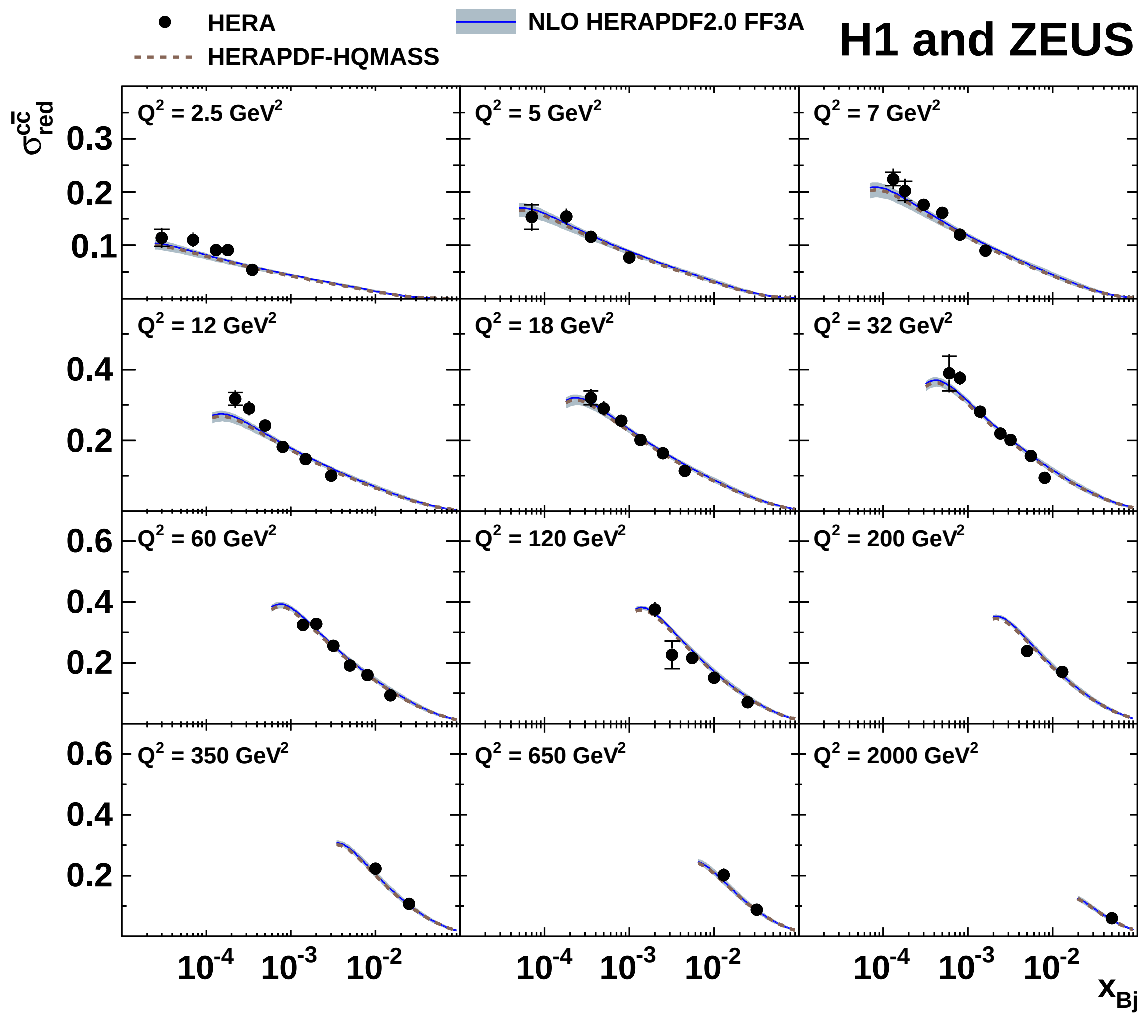

Figure 14: Combined reduced charm cross sections, $\sigma_{\rm red}^{c\bar{c}}$, (full circles) as a function of $x_{\rm Bj}$ for given values of Q^2, compared to the NLO QCD FFNS predictions based on HERAPDF-HQMASS (dashed lines) and on HERAPDF2.0 FF3A (solid lines). The shaded bands on the HERAPDF2.0 FF3A predictions show the theory uncertainties obtained by adding PDF, scale and charm quark mass uncertainties in quadrature.

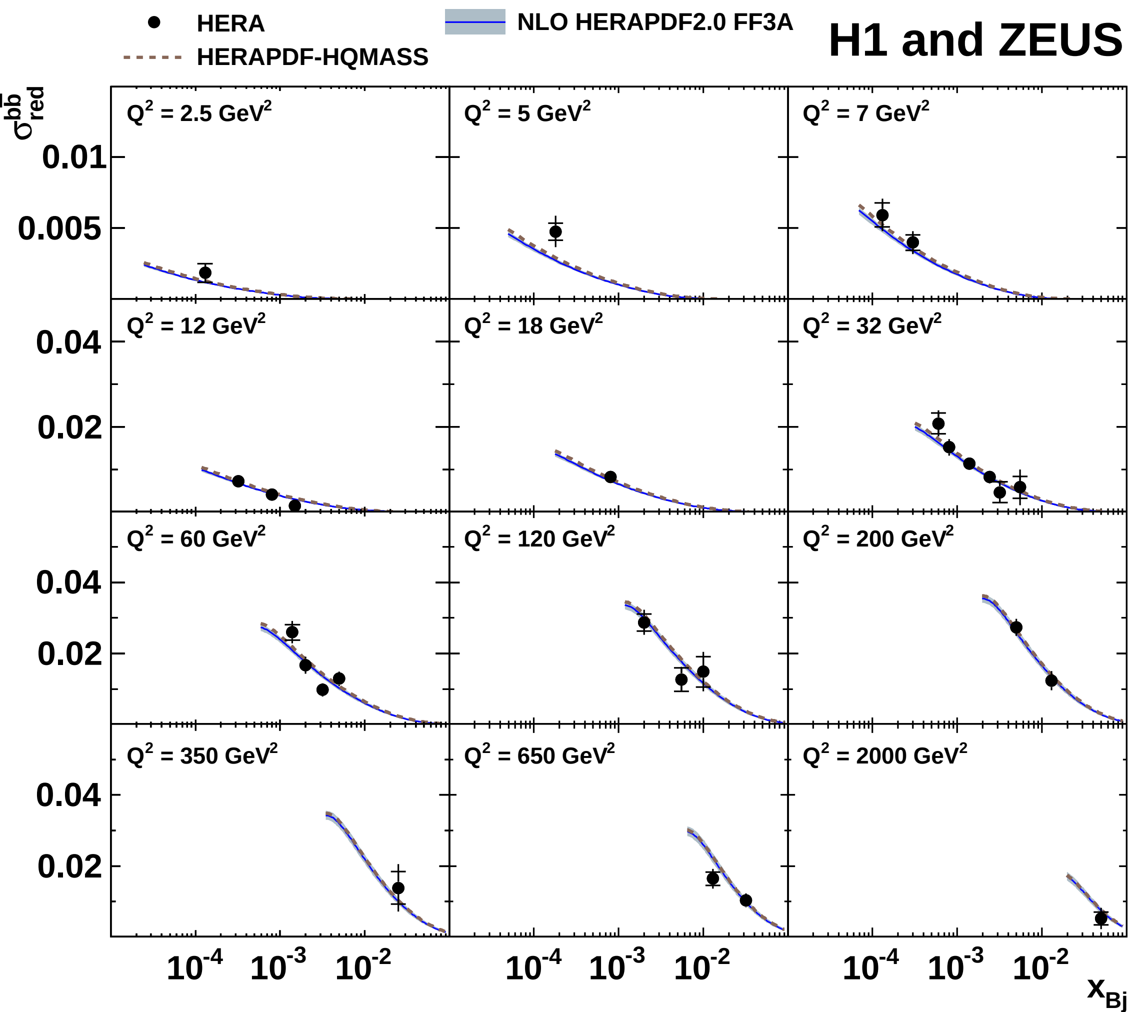

Figure 15: Combined reduced beauty cross sections, $\sigma_{\rm red}^{b\bar{b}}$, (full circles) as a function of $x_{\rm Bj}$ for given values of Q^2, compared to the NLO QCD FFNS predictions based on HERAPDF-HQMASS (dashed lines) and on HERAPDF2.0 FF3A (solid lines). The shaded bands on the predictions using the fitted PDF set show the theory uncertainties obtained by adding PDF, scale and charm quark mass uncertainties in quadrature.

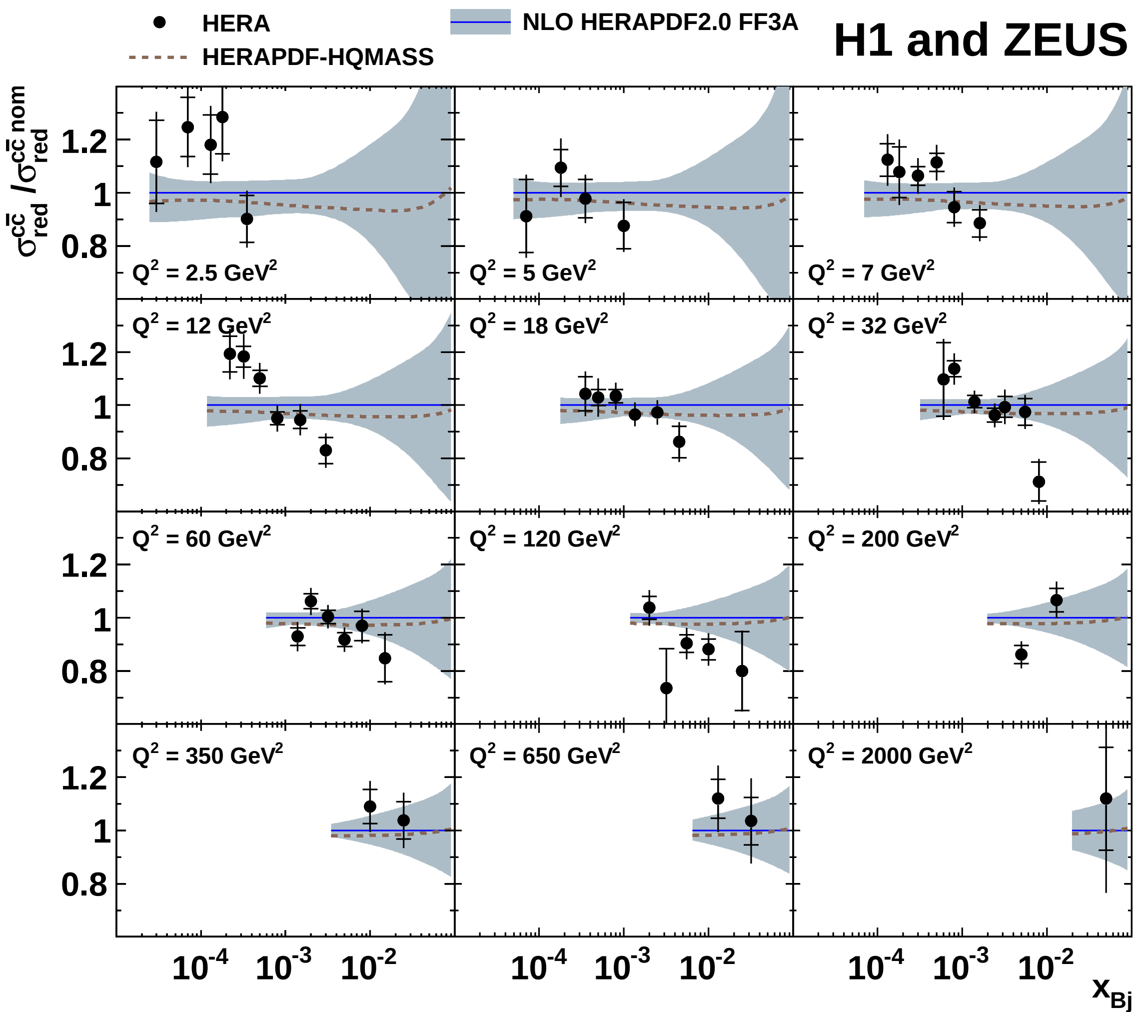

Figure 16: Combined reduced charm cross sections, $\sigma_{\rm red}^{c\bar{c}}$, (full circles) as a function of $x_{\rm Bj}$ for given values of Q^2, compared to the NLO FFNS predictions using HERAPDF-HQMASS (dashed lines), normalised to the reference cross sections using HERAPDF2.0 FF3A (solid lines with uncertainty bands).

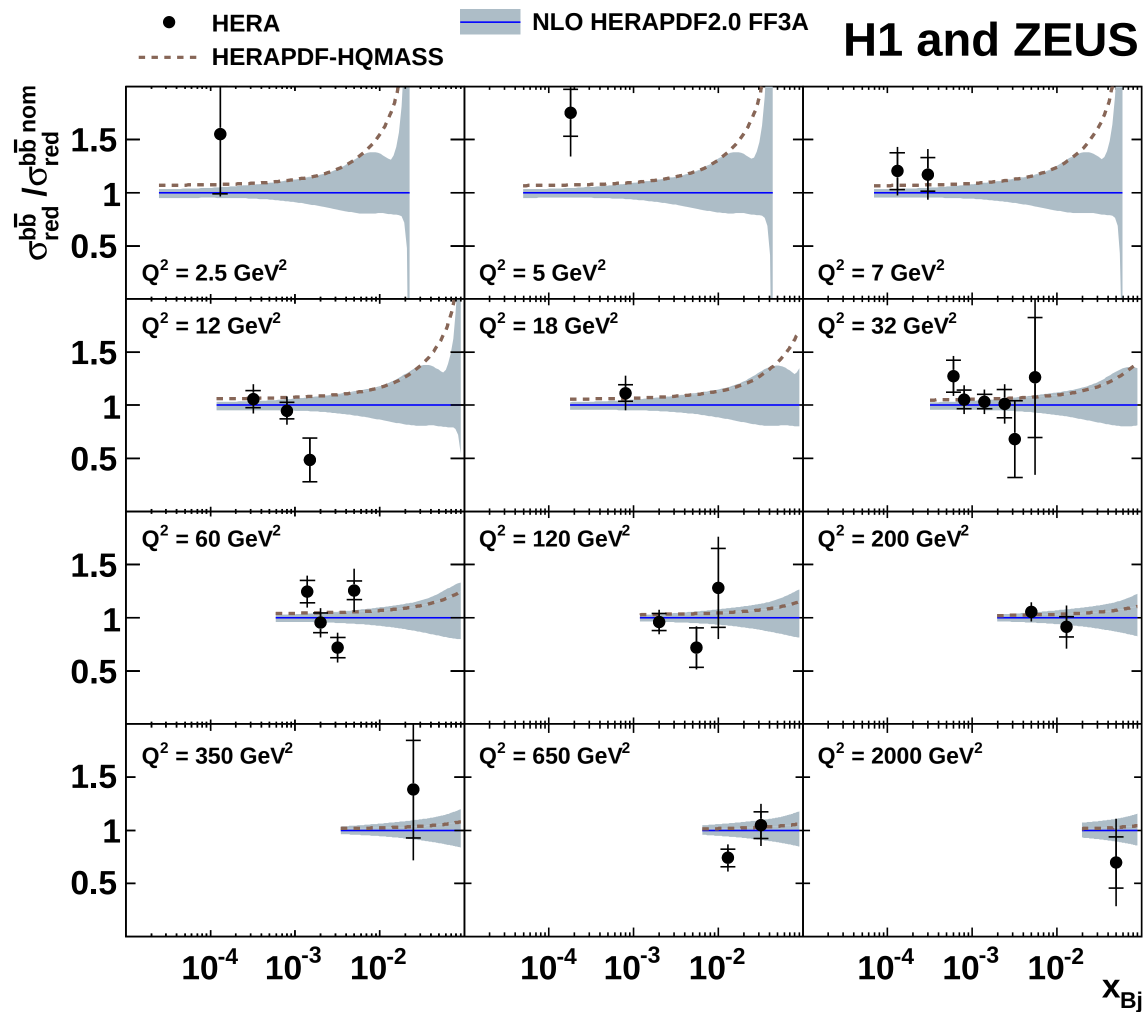

Figure 17: Combined reduced beauty cross sections, $\sigma_{\rm red}^{b\bar{b}}$, (full circles) as a function of $x_{\rm Bj}$ for given values of Q^2, compared to the NLO FFNS predictions using HERAPDF-HQMASS (dashed lines), normalised to the reference cross sections using HERAPDF2.0 FF3A (solid lines with uncertainty bands).

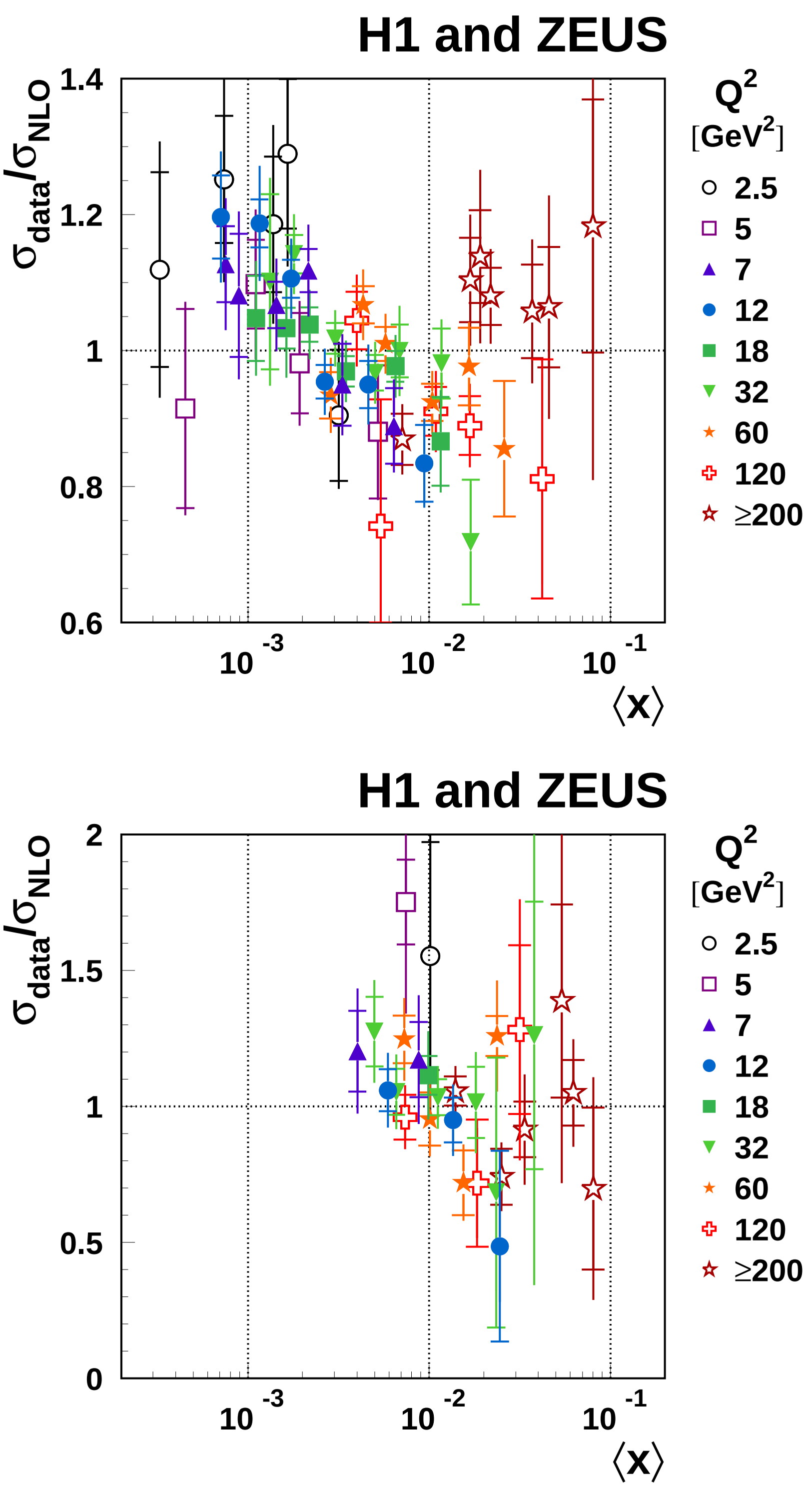

Figure 18: Ratio of the combined reduced cross sections, $\sigma_{\rm red}^{c\bar{c}}$ (a) and $\sigma_{\rm red}^{b\bar{b}}$ (b), to the NLO FFNS cross section predictions, based on HERAPDF-HQMASS, as a function of the partonic $\langle x \rangle$ for different values of Q^2.

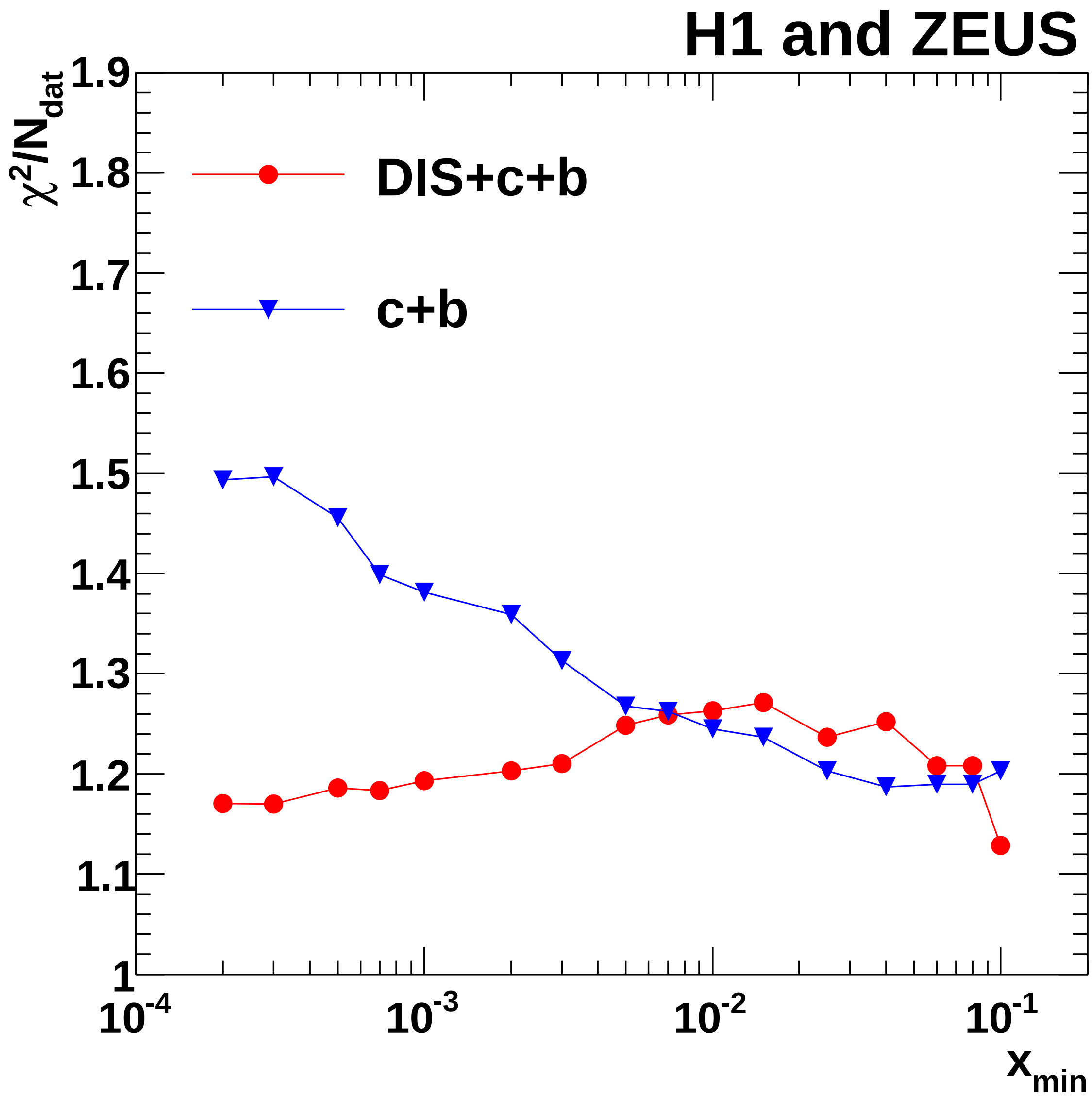

Figure 19: The values of χ^2 divided by the number of data point (N_{dat}) of the QCD fit to the inclusive and heavy flavour data: (triangles) for the heavy flavour data only and (dots) for the inclusive plus heavy flavour data when including in the fit only inclusive data with $x_{Bj} \geq x_{min}$.

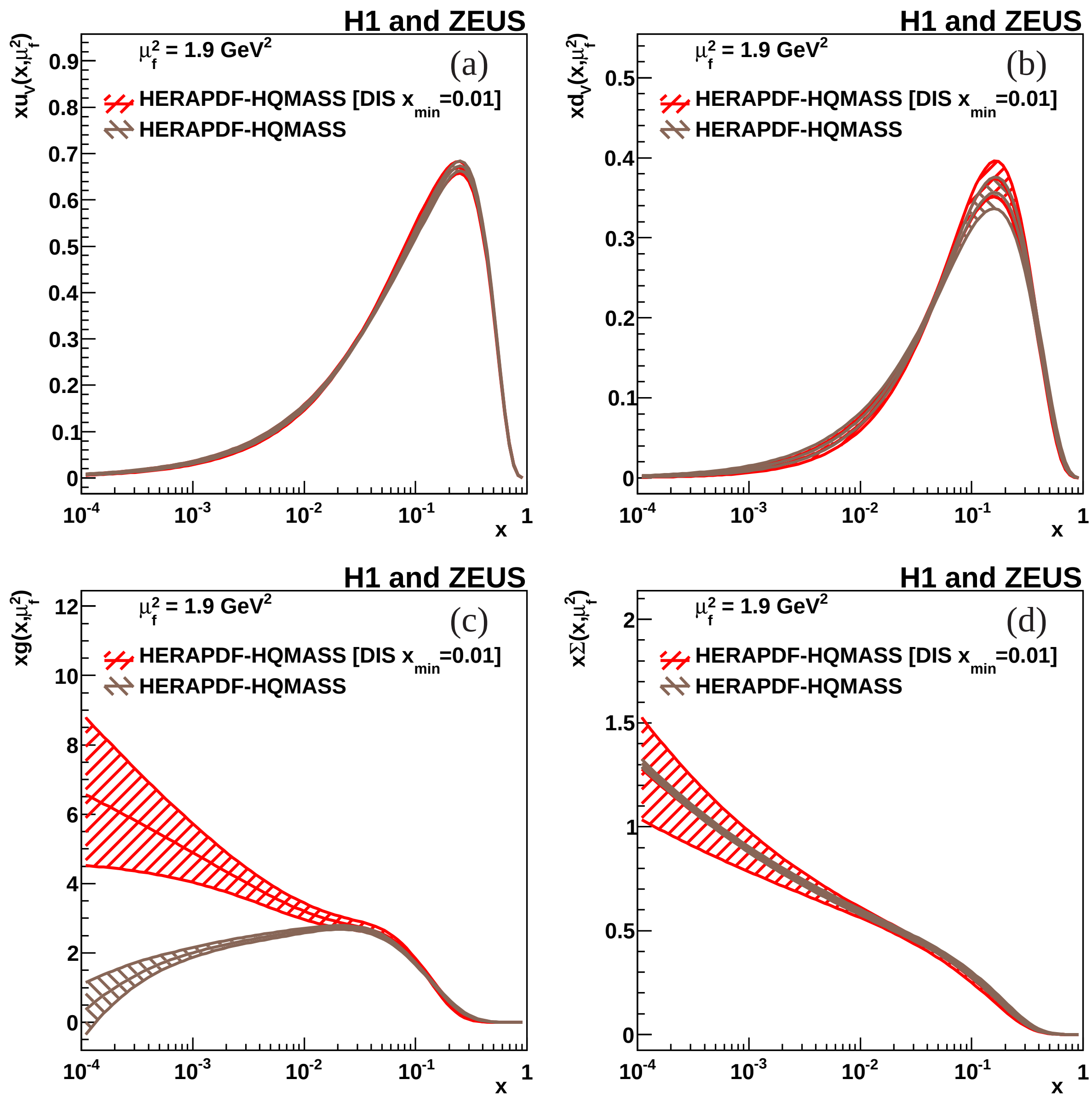

Figure 20: Parton density functions $x \cdot f(x,Q^2)$ at the starting scale $Q_0^2 = 1.9$ GeV^2 with $f = u_v, d_v, g, \Sigma$ for the valence up quark (a), the valence down quark (b), the gluon (c) and the sea quarks (d) of HERAPDF-HQMASS (full lines) and obtained from the QCD fit to the combined inclusive and heavy flavour data with imposing a minimum cut of $x_{\mathrm{Bj}} \geq 0.01$ to the inclusive data included in the fit. The experimental/fit uncertainties are shown by the hatched bands.

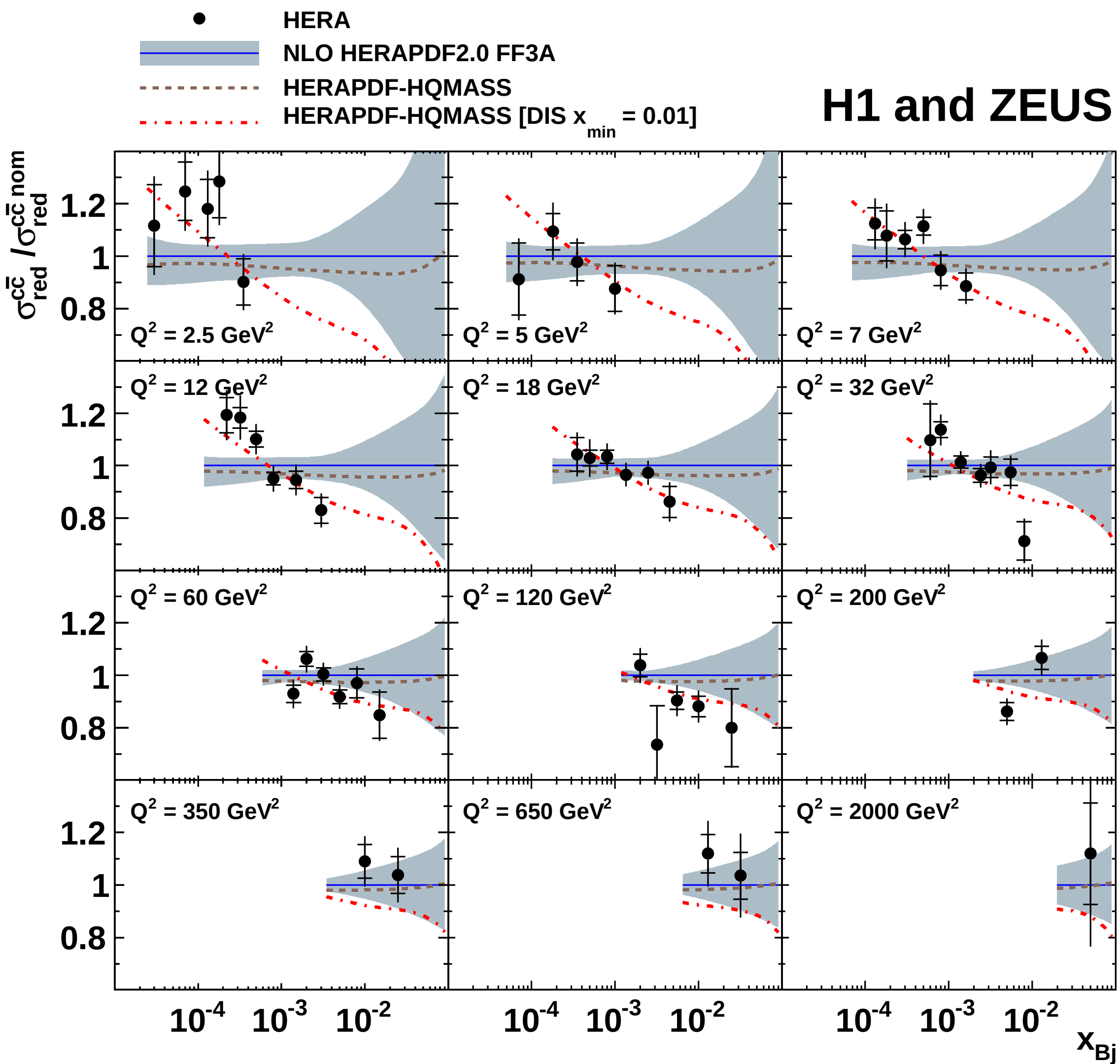

Figure 21: Combined reduced charm cross sections, $\sigma_{\rm red}^{c\bar{c}}$, (full circles) as a function of $x_{\rm Bj}$ for given values of Q^2, compared to the NLO FFNS predictions based on HERAPDF-HQMASS (dashed lines) and those resulting from the alternative fit when requiring $x_{\rm Bj} \geq 0.01$ for the inclusive data (dashed dotted lines, normalised to the reference cross sections using HERAPDF2.0 FF3A (full line). The experimental/fit uncertainties of the reference cross sections are indicated by the shaded bands.

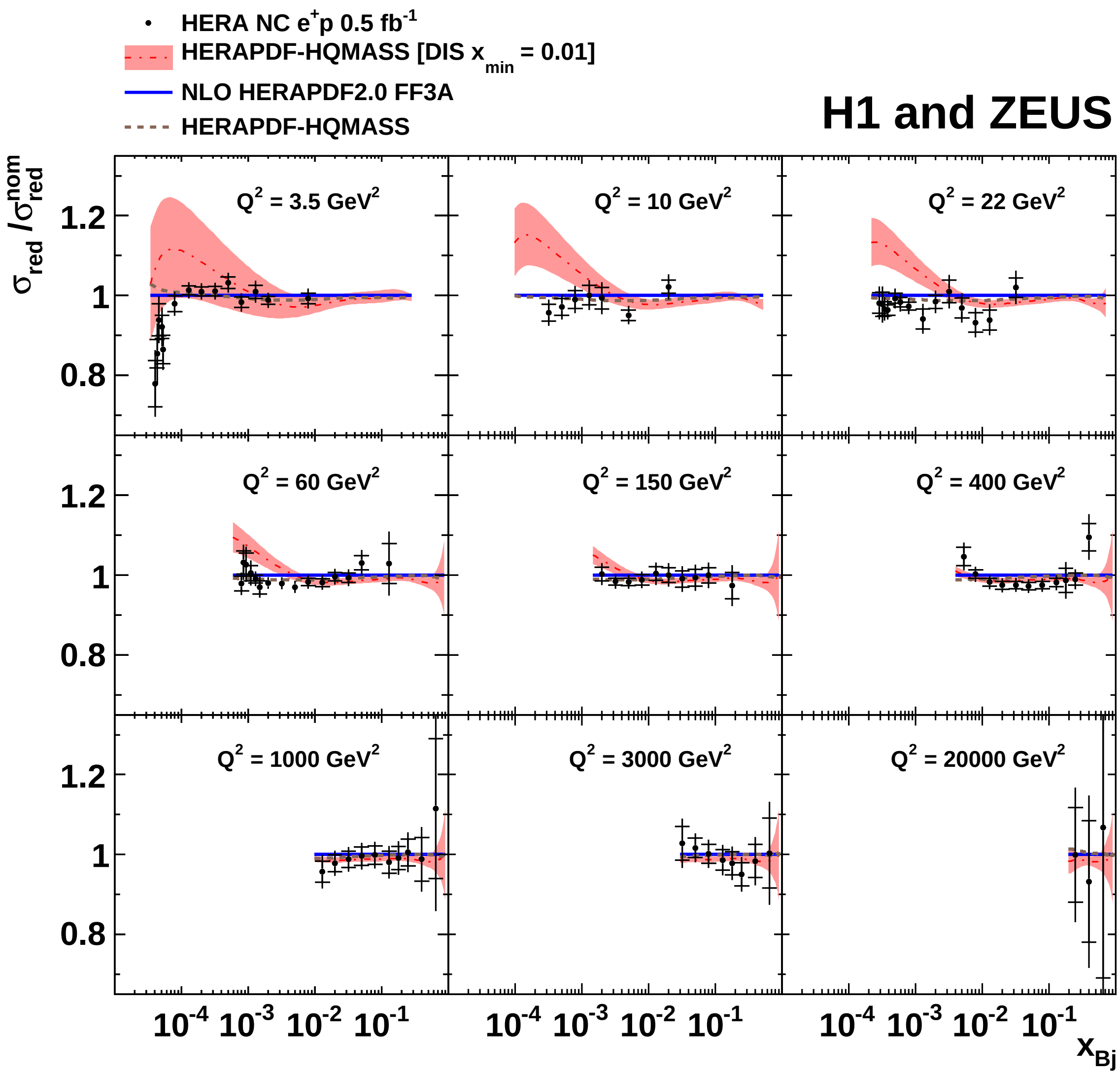

Figure 22: Combined reduced NC cross sections, $\sigma_{\rm red}$, (full circles) as a function of $x_{\rm Bj}$ for selected values of Q^2, compared to the NLO FFNS predictions based on HERAPDF-HQMASS (dashed lines) and those resulting from the alternative fit with $x_{\rm Bj} \geq 0.01$ required for the inclusive data (dashed-dotted lines), normalised to the reference cross sections using HERAPDF2.0 FF3A (solid lines).

Appendix

Table A.1 lists the sources of correlated uncertainties together with the shifts and reductions obtained as a result of the combination. Table A.2 provides the input parameters for the HERAPDF-HQMASS fit and the variations considered to evaluate model and parameterisation uncertainties. Table A.3 provides the central values of the fitted parameters.

Data set	Name	shift [σ]	reduction factor
2–7,8c,9,10,11c,	theory, m_c	0.29	0.65
2–13	theory μ_r, μ_f variation	–0.82	0.45
2–13	theory, $\alpha_S(M_Z)$	0.17	0.95
1–7,8c,9,10	theory, c fragmentation α_K	–0.82	0.80
2–7,8c,9,10	theory, c fragmentation $\hat{s}$	–1.44	0.83
2–7,8c,9,10	theory, c transverse fragmentation	–0.10	0.90
2–7,10	$f(c \to D^{*+})$	0.43	0.92
2–6,10	$BR(D^{*+} \to D^0\pi^+)$	0.14	0.99
2–7,10	$BR(D^0 \to K^-\pi^+)$	0.47	0.98
1–4	H1 CJC efficiency	0.29	0.78
2	H1 integrated luminosity (1998-2000)	–0.05	0.97
2	H1 trigger efficiency (HERA-I)	–0.07	0.94
2–4	H1 electron energy	0.29	0.67
2–4	H1 electron polar angle	0.23	0.74
2	H1 MC alternative fragmentation	–0.09	0.68
3,4	H1 primary vertex fit	0.31	0.98
1,3,4	H1 hadronic energy scale	–0.06	0.81
3,4	H1 integrated luminosity (HERA-II)	–0.19	0.77
3,4	H1 trigger efficiency (HERA-II)	–0.06	0.98
3,4	H1 fragmentation model in MC	–0.17	0.87
1,3,4	H1 photoproduction background	0.31	0.91
3,4	H1 efficiency using alternative MC model	0.30	0.71
1	H1 vertex resolution	–0.53	0.88
1	H1 CST efficiency	–0.34	0.89
1	H1 B multiplicity	0.26	0.79
1	H1 D^+ multiplicity	–0.30	0.94
1	H1 D^{*+} multiplicity	–0.02	0.98
1	H1 D_s^+ multiplicity	0.09	0.97

Table A.1: Sources of bin-to-bin correlated systematic uncertainties considered in the combination. For each source, the affected datasets are given, together with the cross section shift induced by this source and the reduction factor of the correlated uncertainty in units of σ after the first iteration. For those measurements which have simultaneously extracted beauty and charm cross sections, a suffix b or c indicates that the given systematic source applies only to the beauty or charm measurements, respectively.

Data set	Name	shift $[\sigma]$	reduction factor
1	H1 b fragmentation	-0.05	0.96
1	H1 VTX model: x reweighting	-0.20	0.92
1	H1 VTX model: p_T reweighting	-0.31	0.68
1	H1 VTX model: $\eta(c)$ reweighting	-0.36	0.80
1	H1 VTX uds background	-0.14	0.43
1	H1 VTX ϕ of c quark	0.05	0.84
1	H1 VTX F_2 normalisation	-0.05	0.93
9,10,11	ZEUS integrated luminosity (HERA-II)	-1.24	0.88
9,10,11	ZEUS tracking efficiency	0.03	0.88
11	ZEUS VTX decay length smearing (tail)	-0.23	0.96
9,10,11	ZEUS hadronic energy scale	0.08	0.54
9,10,11	ZEUS electron energy scale	0.24	0.55
11	ZEUS VTX Q^2 reweighting in charm MC	-0.10	1.00
11	ZEUS VTX Q^2 reweighting in beauty MC	0.04	1.00
11	ZEUS VTX $\eta(\text{jet})$ reweighting in charm MC	-0.57	0.97
11	ZEUS VTX $\eta(\text{jet})$ reweighting in beauty MC	0.10	0.99
11	ZEUS VTX $E_T(\text{jet})$ reweighting in charm MC	0.48	0.96
11	ZEUS VTX $E_T(\text{jet})$ reweighting in beauty MC	-0.43	0.92
11	ZEUS VTX light-flavour background	0.48	0.85
11	ZEUS VTX charm fragmentation fucntion	-0.91	0.87
11	ZEUS VTX beauty fragmentation fucntion	-0.17	0.95
9	$f(c \to D^+)$	-0.11	0.94
9	$BR(D^+ \to K^-\pi^+\pi^+)$	-0.10	0.95
9	ZEUS D^+ decay length smearing	0.05	0.99
9,10	ZEUS beauty MC normalisation	0.67	0.85
9	ZEUS D^+ η MC reweighting	0.23	0.85
9	ZEUS D^+ p_T, Q^2 MC reweighting	0.92	0.66
9	ZEUS D^+ MVD hit efficiency	-0.04	0.99
9	ZEUS D^+ secondary vertex description	-0.08	0.97
5,13	ZEUS integrated luminosity (1996-1997)	0.57	0.95

Table A.1: continued

Data set	Name	shift $[\sigma]$	reduction factor
6,13	ZEUS integrated luminosity (1998-2000)	0.42	0.87
10	ZEUS D^{*+} $p_T(\pi_s)$ description	0.84	0.92
10	ZEUS D^{*+} beauty MC efficiency	-0.17	0.97
10	ZEUS D^{*+} photoproduction background	0.39	0.96
10	ZEUS D^{*+} diffractive background	-0.35	0.92
10	ZEUS D^{*+} p_T, Q^2 MC reweighting	-0.45	0.91
10	ZEUS D^{*+} η MC reweighting	0.34	0.77
10	ZEUS D^{*+} $\Delta(M)$ window efficiency	-0.77	0.92
7	$f(c \rightarrow D^0)$	0.32	0.99
7,8,12	ZEUS integrated luminosity (2005)	0.66	0.91
8c	$BR(c \rightarrow l)$	-0.10	0.97
8	ZEUS μ: B/RMUON efficiency	0.54	0.90
8	ZEUS μ: FMUON efficiency	0.15	0.95
8	ZEUS μ: energy scale	-0.01	0.67
8	ZEUS μ: p_T^{miss} calibration	0.13	0.66
8	ZEUS μ: hadronic resolution	0.62	0.58
8	ZEUS μ: IP resolution	-0.70	0.83
8	ZEUS μ: MC model	-0.08	0.75
1b	H1 VTX beauty: Q^2 charm reweighting	-0.02	1.00
1b	H1 VTX beauty: Q^2 beauty reweighting	-0.02	0.99
1b	H1 VTX beauty: x reweighting	0.09	0.89
1b	H1 VTX beauty: p_T reweighting	-1.06	0.82
1b	H1 VTX beauty: η reweighting	0.01	0.91
1b	H1 VTX beauty: BR(D^+)	-0.21	0.99
1b	H1 VTX beauty: BR(D^0)	0.16	1.00
8b,11b,12,13	theory, m_b	0.60	0.93
8b,12,13	theory, b fragmentation	-0.71	0.97
8b,12,13,	$BR(b \rightarrow l)$	-0.60	0.97
13	ZEUS muon efficiency (HERA-I)	-1.02	0.91

Table A.1: continued

Variation	Standard Value	Lower Limit	Upper Limit
$Q^2_{\min}$ [GeV^2]	3.5	2.5	5.0
f_s	0.4	0.3	0.5
$\alpha_s^{n_f=3}(M_Z)$	0.106	0.1045	0.1075
$\mu^2_{r,f}$	$Q^2+4m^2_{\mathrm{Q}}$	$0.25\cdot(Q^2+4m^2_{\mathrm{Q}})$	$4\cdot(Q^2+4m^2_{\mathrm{Q}})$
$\mu^2_{\mathrm{f},0}$ [GeV^2]	1.9	1.6	2.2

Table A.2: Input parameters for the HERAPDF-HQMASS fit and the variations considered to evaluate model and parametrisation ($\mu^2_{\mathrm{f},0}$) uncertainties.

	A	B	C	D	E	A'	B'
xg	2.81	-0.198	8.14			1.39	-0.273
xu_v	3.66	0.678	4.87		14.7		
xd_v	3.38	0.820	4.27				
$x\overline{U}$	0.102	-0.172	8.27	13.9			
$x\overline{D}$	0.170	-0.172	5.83				
$m_c(m_c)$ [GeV]	1.29						
$m_b(m_b)$ [GeV]	4.05						

Table A.3: Central values of the fitted parameters of HERAPDF-HQMASS.